CENTER FOR INFRASTRUCTURE ENGINEERING STUDIES

DESTRUCTIVE AND NON-DESTRUCTIVE TESTING OF BRIDGE J857 PHELPS COUNTY, MISSOURI

VOLUME II

FEASIBILITY STUDY ON DAMAGE DETECTION OF RC STRUCTURES USING DYNAMIC SIGNATURE TESTS

by

Genda Chen

Xinbao Yang

Huimin Mu

Antonio Nanni

University of Missouri-Rolla

CIES 99-08B

Technical Report Documentation Page

1. Report No. RDT01-002B	**2. Government Accession No.**	**3. Recipient's Catalog No.**
4. Title and Subtitle Destructive and Non-Destructive Testing of Bridge J857, Phelps County, Missouri Volume I - Strengthening and Testing to Failure of Bridge Decks Volume II – Feasibility Study on Damage Detection of RC Structures Using Dynamic Signature Tests Volume III-Strengthening and Testing to Failure of Bridge Piers		**5. Report Date** April, 2001 **6. Performing Organization Code** UMR
7. Author/s T. Alkhrdaji, M. Barker, G. Chen, H. Mu, A. Nanni, and X. Yang		**8. Performing Organization Report No.** RDT01-002B/RI98-013
9. Performing Organization Name and Address Center for Infrastructure Engineering Studies University of Missouri at Rolla 223 ERL Rolla, MO 65409-0710		**10. Work Unit No. (TRAIS)** **11. Contract or Grant No.**
12. Sponsoring Organization Name and Address MoDOT Research Development and Technology 1617 Missouri Blvd., Jefferson City, MO 65101 University Transportation Center - UMR 223 Engineering Research Lab., Rolla, MO 65409		**13. Type of report and period covered** Technical Report; 10/98 – 9/99 **14. Sponsoring Agency Code** MoDOT

15. Supplementary Notes
This investigation was conducted in cooperation with the U.S. Department of Transportation.

16. Abstract
This report presents the results of a research program aimed at investigating the constructability and effectiveness of externally bonded FRP strengthening systems for improving the flexural capacity of bridge decks and piers. The joint effort of two universities, industry, and a state DOT provided the premise for a successful outcome. Bridge J857 was constructed in 1932 and was scheduled for demolition in the fall of 1998 due to highway realignment. Two of the three solid reinforced concrete (RC) decks were strengthened using two FRP systems namely, near-surface mounted carbon FRP (CFRP) rods and surface bonded CFRP sheets. Bridge decks were tested to failure under quasi-static loading cycles. Flexural strengthening of bridge columns was achieved by mounting CFRP rods on two opposite sides of the columns. Columns were also jacketed with carbon and glass FRP laminates. The experimental moment capacities of the decks compared well with theoretical values. Strengthened decks exhibited ductile behavior prior to FRP failure. The columns were tested to failure by applying lateral load cycles. The proposed strengthening technique for the bridge columns is feasible and effective for improving the flexural capacity of RC columns. The capacity of the strengthened column sections could be predicted using classical methods of analysis. Dynamic tests were conducted on the deck strengthened with CFRP sheets. The objective of dynamic tests was to relate the change in fundamental frequency to the induced damage, which could be used as a tool to assess the damage level of RC structural members. An effective damage indicator was identified that requires no baseline for damage level detection.

17. Key Words bridge, fiber reinforced polymer, pier, deck, solid slabs, strengthening	**18. Distribution Statement** No restrictions. This document is available to the public through NTIC, Springfield, VA 22161		
19. Security Classification (of this report) Unclassified	**20. Security Classification (of this page)** Unclassified	**21. No. of Pages** 93	**22. Price**

Form DOT F 1700.7 (8-72) Reproduction of form and completed page is authorized.

Disclaimer

The contents of this report reflect the views of the author(s), who are responsible for the facts and the accuracy of information presented herein. This document is disseminated under the sponsorship of the Center for Infrastructure Engineering Studies (CIES), University of Missouri -Rolla, in the interest of information exchange. CIES assumes no liability for the contents or use thereof.

The mission of CIES is to provide leadership in research and education for solving society's problems affecting the nation's infrastructure systems. CIES is the primary conduit for communication among those on the UMR campus interested in infrastructure studies and provides coordination for collaborative efforts. CIES activities include interdisciplinary research and development with projects tailored to address needs of federal agencies, state agencies, and private industry as well as technology transfer and continuing/distance education to the engineering community and industry.

Center for Infrastructure Engineering Studies (CIES)
University of Missouri-Rolla
223 Engineering Research Lab
1870 Miner Circle
Rolla, MO 65409-0710
Tel: (573) 341-6223; fax -6215
E-mail: cies@umr.edu
www.umr.edu/~cies

DESTRUCTIVE AND NON-DESTRUCTIVE TESTING OF BRIDGE J857 PHELPS COUNTY, MISSOURI VOLUME II FEASIBILITY STUDY ON DAMAGE DETECTION OF RC STRUCTURES USING DYNAMIC SIGNATURE TESTS

EXECUTIVE SUMMARY

Dynamic signature tests have been widely used in aerospace and mechanical engineering to detect damage in aircrafts and mechanical systems. Their applications to the reinforced concrete (RC) structures in civil engineering, especially full-scale or prototype concrete structures, have a more recent origin. In this report, this technique is further verified by statically and dynamically testing in parallel three full-scale RC beams and a solid deck of Bridge J857 in Missouri. A new damage indicator is developed specifically for use in RC structures. The relation in transfer functions between harmonic and swept-sine tests is studied extensively so that a single swept-sine test can be used to represent a series of harmonic tests.

Emphasis is placed upon the fundamental frequency and modal damping in this study. They are identified from the transfer functions of deflection and/or acceleration of RC structures, representing the relation between a response quantity and the excitation frequency in harmonic tests. Damage was introduced by applying a concentrated load at midspan of a simply supported beam or bridge deck with a hydraulic actuator. Forced vibration tests with a mechanical oscillator were conducted to obtain various transfer functions. Each test was performed under a sinusoidal load of one excitation frequency. Surprisingly, it was observed from laboratory tests that a transfer function determined from a series of harmonic tests with the excitation frequency increasing in sequence considerably differs from the one with the excitation frequency decreasing when a RC specimen under testing cracks severely. The resonant frequency significantly shifts from one case to another even though both are evaluated for one state of damage in the specimen. Furthermore, the shift in resonant frequency disappeared after the specimen was subjected to vibration up to about half an hour and therefore represented the transient property of a newly damaged specimen. The maximum shift in resonant frequency happens at the beginning of dynamic tests and is well correlated with the severity of damage. Thus, the frequency shift is an effective damage indicator resulting from this study, which requires no baseline to detect damage. In addition, the frequency shift mainly reflects the unstable surface condition along cracks and therefore is significantly more sensitive to the location of damage than the commonly used indicator --- change in natural frequency from one damage state to another. Together with the change in natural frequency, the frequency shift may provide a viable tool in detecting the severity and localization of damage in concrete structures.

Due to repetitious work and time-consuming effort to determine a transfer function using harmonic tests, the behaviors of RC structures under swept-sine loads are studied in great detail. The excitation frequency in swept-sine loads is considered to be linearly increasing and then decreasing with time. When the frequency rate of the increasing or decreasing range is sufficiently high, the beating phenomenon appears immediately after the resonance. To avoid the occurrence of the beating phenomenon and ensure the accuracy in determining the natural frequency of a RC structure, it is recommended that the frequency rate be limited less than $f_1^2/2000$ in which f_1 is the fundamental frequency of the structure. Based on analytical study, the resonant frequency, resonant acceleration and damping ratio determined from harmonic tests are respectively related to those from swept-sine tests. These relations are validated using experimental data and show reasonable accuracy in predicting the quantity of interest corresponding to harmonic tests.

The final report consists of three volumes. The current Volume (Volume II) focuses on the laboratory and field dynamic tests. Volume I focuses on the strengthening and testing to failure of the three decks of the bridge. Volume III focuses on the strengthening and testing to failure of the bridge piers.

ACKNOWLEDGEMENTS

The research program was made possible with the financial support received from the Missouri Department of Transportation, Mid-America Transportation Center, University of Missouri-Rolla/University Transportation Center on Advanced Materials and NDT Technologies. Master Builders Technologies, Cleveland, OH, and Structural Preservation Systems, Baltimore, MD, provided and installed the FRP systems, respectively. Chester Bross Construction Company, Hannibal, MO, was the general contractor.

The authors would like to express their sincere thanks to the graduate students: Jingning Wu, Tarek Alkhrdaji, Chaoqiang Chen for their help during the laboratory and field tests. Thanks are also extended to Jeef Bradshaw, P.E., UMR, Professor Michael Barker, UMC, and C. H. Cassil for their assistance in the bridge tests.

The results, opinions and conclusions expressed in this report are solely those of the authors and do not necessarily represent those of the sponsors.

TABLE OF CONTENTS

LIST OF ILLUSTRATIONS

LIST OF TABLES

NOTATION

a = height of stress block (in).
A_s = area of tension reinforcement (in^2).
A_h =Constant load amplitude under harmonic tests (lb).
b = width of beam (in).
c = height of neutral axis (in) or phase difference between a swept-sine and a sinusoidal load (lb).
C = compress force (lb).
d = distance from the extreme compression side to the centroid of tension reinforcement (in).
E = modulus of elasticity (psi).
E_s = modulus of elasticity of steel (psi).
f = Excitation frequency of shaker (Hz).
f_1 = fundamental engineering frequency or frequency corresponding to lower bound of 50% power in halfpower method (Hz).
f_2 = frequency corresponding to higher lower bound of 50% power in halfpower method (Hz).
f_n =Resonant frequency obtained fromtransfer function (Hz).
f_c' = compressive strength of concrete (psi).
f_p = engineering frequency of beam with preload (Hz).
f_r = modulus of rupture of concrete (psi).
f_s = stress in tension reinforcement (psi).
f_{swept} = Resonant frequency of a beam identified with a swept-sine test (Hz).
f_{sine} = Resonant frequency under harmonic loads or natural frequency of the beam (Hz).
f_y = yielding strain of steel rebars (psi).
g = gravitational acceleration (386.0 in/sec^2).
h = height of beam (in).
I = moment of inertia of uncracked beam cross section (in^4).
I_{cr} = moment of inertia of transferred cross section (in^4).
I_e = effective moment of inertia of beam cross section (in^4).
I_g = moment of inertia of gross section of beam (in^4).
k = stiffness constant of simply supported beam (in/lb).
L = length of beam (ft).
M_a = applied moment on beam by static load (k-ft).
M_{cr} = cracking moment of beam section (k-ft).
M_p = mass of preload ($lb.sec^2/in$).
M_u = moment strength of beam section (k-ft).
MF = modification factor of load amplitude under swept-sine tests.
P_0 = amplitude of force induced by shaker (lb).
P_{pre} = preload (lb).

P_s = static load applied on beam (kips).
P_{ser} = service load of bridge deck (lb).
$P(t)$ = Swept-sine dynamic load (lb).
P_u = load carrying capacity of beam (kips).
Q = quality factor in halfpower method.
r' = Increasing or decreasing rate of the operating frequency (Hz/sec).
r = Increasing or decreasing rate of the excitation frequency (Hz/sec).
t = Time (sec).
T = tension force (lb).
W = weight of beam (lb).
W_p = weight of lumped mass (preload) (lb).
y_D =dynamic deflection of beam (in).
$y_{D\max}$ = maximum deflection of beam (in).
$\ddot{y}_{D\max}$ = maximum acceleration of beam (in/sec^2).
α = crack related constant.
δA = Relative error in resonant acceleration.
δf = Relative error in resonant frequency.
$\delta\zeta$ = Relative error in damping ratio.
ε_{cu} = ultimate strain of concrete (in/in).
ε_s = strain in tension reinforcement (in/in).
θ = angle between eccentric masses (rad).
ξ = damping ratio.
ρ = mass of beam per unit length (lb.sec^2/in^2).
ϕ = phase angle (rad).
ω_1 = fundamental circular frequency (rad/sec).
Ω = applied frequency of shaker (rad/sec).
Δf = frequency shift (Hz).
Φ_1 = mode shape.

1. INTRODUCTION

During its service life, a transportation structure may be subject to damage in addition to aging deterioration. The damage may result from overloading, truck collision or natural effects such as tornadoes and earthquakes (Doebling, *et al* 1996, Chang, 1997, Sanayei, 1991). Detection of damage in a structure can help engineers more accurately assess the structure condition immediately after an accident or make a proper decision whether to retrofit or replace the damaged structure. Among various detection techniques, the dynamic signature test is one of the most popular nondestructive evaluation methods, especially in mechanical and aerospace engineering (Yao, 1992, Stubbs, 1987, Schulz, 1996). It can detect the global damage occurring in a structure and sometimes locate the damage area without interrupting the normal operation of the structure.

The existence of damage in structures will modify the vibrational characteristics of the structures such as natural frequencies, mode shapes and modal damping ratio. These parameters can be extracted from the structural dynamic responses of model tests (Ewins, 1984, Salawu, 1995). Their differences between two consecutive tests reflect possible damage in the structures during the interval period and may be used to identify the severity of damage and location. A series of repeated dynamic tests over several years for the purposes of identifying any damage in structures are referred to as the dynamic signature tests in this report. Among the various parameters, the natural frequency is widely used as a reliable indicator of damage occurring in a structure since it can be readily identified from model tests. If damage occurs in a structure, stiffness degradation will take place, which accordingly causes the change of resonant frequencies for various modes. The significant reduction in stiffness can be inferred when the measured resonance frequencies are substantially lower than the baseline values (usually defined as frequencies in the undamaged state). A minimum of 5% change in frequency is necessary to draw a convincing conclusion (Salawu, 1997).

The fundamental frequency tends to capture the global changes in a structure and is less sensitive to local modification to the structure. Since the global changes are often related to the structural integrity, the change in fundamental frequency can thus be used to assess the structural safety. Damage may be located in conjunction with other methods, such as the acoustic emission, ultrasonic, magnetic particle, and the eddy-current method.

The objective of this project is to verify the feasibility of using dynamic signature tests to assess the condition of reinforced concrete (RC) structures unstrengthened and strengthened with externally bonded CFRP sheets. Static and dynamic tests are conducted in parallel on three reinforced concrete beams in lab. The deflection and acceleration time history responses at different points of the beam are recorded when the beams are subjected to harmonic loads of various frequencies. These responses are then processed to extract the transfer functions, from which the resonant frequencies and damping ratios are determined. To expedite the process of dynamic tests, swept-sine tests are also carried out and their results are compared with the harmonic tests. Change in frequency before and after a static load is applied is correlated with the severity of damage, which is represented by the static load in this study.

2. THEORETICAL BACKGROUND ON DYNAMIC TESTS

2.1. FUNDAMENTAL FREQUENCY OF SIMPLY-SUPPORTED BEAMS

The fundamental frequency and mode shape of a uniform, simply-supported beam can be formulated as follows (Thompson, 1985):

$$\omega_1 = (\frac{\pi}{L})^2 \sqrt{\frac{EI}{\rho}} \quad \text{(rad/sec)} \tag{2.1}$$

$$\Phi_1(x) = \sin\frac{x\pi}{L} \tag{2.2}$$

where ρ is the mass density of the beam per unit length (lb.sec^2/in^2), E is the modulus of elasticity of concrete (=57000$\sqrt{f_c^{'}}$ psi), I is the moment of inertia of the cross section of the beam, L denotes the span length, and $f_c^{'}$ represents the compressive strength of concrete. The engineering frequency $f_1 = \frac{\omega_1}{2\pi}$ with a unit of Hz.

For the unstrengthened beam to be discussed in Section 3.1, L=19.0 ft, I=7914.5 in^4, $f_c^{'}$=5770 psi, and ρ=0.06114 lb.sec^2/in^2. The fundamental frequency of the beam can then be determined from Eq. (2.1) as f_1=22.3 Hz.

When a lumped mass M_p is attached at midspan of the beam, the fundamental frequency of the beam plus the mass can be expressed into (Thompson, 1985):

$$f_p = \frac{f_1}{\sqrt{1+2M_p/(\rho L)}} = \frac{f_1}{\sqrt{1+2W_p/W}} \tag{2.3}$$

in which W_p and W denote the weight of the lumped mass and the weight of the beam respectively.

2.2. DYNAMIC LOAD

The dynamic load used for the test of the beams was induced by a mechanical oscillator (shaker). The shaker utilizes the centrifugal force of two unbalanced masses to generate a variable force which can be expressed into:

$$P(t) = P_0 \sin\Omega t\ . \tag{2.4}$$

In the equation above, Ω is the forcing frequency in rad/sec and P_0 represents the amplitude of the force which can be further determined by:

$$P_0 = 0.03 \times 4\pi^2 \times f^2 \times \sin(\theta/2)\ \text{lb} \tag{2.5}$$

The quantity θ in Eq.(2.5) is the angle between eccentric masses and f is the operating speed of the shaker in cycles per second. When the shaker is operated at a constant speed, $\Omega=2\pi f$.

During the dynamic tests, a RC beam vibrates up and down periodically. To prevent it from jumping, the beam shall always be in contact with its supports for the entire duration of dynamic tests. This can be guaranteed by limiting the dynamic acceleration within the level of the gravitational acceleration.

The midspan deflection of the beam (first mode approximation) under the dynamic load described in Eq. (2.4) can be calculated from:

$$y_D = \frac{P_0 \sin(\Omega t + \phi)/k}{\sqrt{(1-\frac{\Omega^2}{\omega_1^{\,2}})^2 + (\frac{2\xi\Omega}{\omega_1})^2}} \tag{2.6}$$

where ξ is the damping ratio of the beam, ϕ is the phase angle of the deflection with respect to the dynamic load, and k denotes the stiffness of the beam at midspan equal to $48\frac{EI}{L^3}$. At resonance, $\Omega = \omega_1$. The maximum deflection amplitude can therefore be simplified into:

$$y_{D\max} = \frac{P_o}{k} \times \frac{1}{2\xi} \ . \tag{2.7}$$

Correspondingly, the maximum acceleration is equal to:

$$\ddot{y}_{D\max} = \Omega^2 y_{D\max} = \frac{P_o}{k} \times \frac{\omega_1^2}{2\xi} . \tag{2.8}$$

To avoid the beam's uplifting from its supports, the maximum acceleration must be less than the gravitational acceleration. That is:

$$\ddot{y}_{D\max} \le g \tag{2.9}$$

or

$$P_0 \le 2\xi kg/\omega_1^2 . \tag{2.10}$$

It is anticipated that the largest acceleration of a beam occurs when the beam behaves elastically or experiences minor cracking. Therefore, it is reasonable to assume 2% of critical damping to estimate the amplitude of dynamic loads. Under these circumstances, $P_0 \le 2*0.02*136610*386/140.2^2 = 108.0$ lb. For the harmonic tests of the RC beams in this study, P_0=92.89 lb was used which corresponds to $\theta = 18^\circ$ at resonance.

2.3. THE CONCEPT OF PRELOAD

Flexural and shear cracks develop in a RC beam when subjected to high tensile stresses. It is likely that a cracked beam under dynamic loads vibrates in a nonlinear fashion due to the close-and-open nature of cracks. For consistent test results and the ease of interpreting the test data using the linear vibration theory, the concept of preloading the beam is introduced. The effect of the preload is to keep the cracks open during the entire period of the dynamic tests.

The level of preload is determined based on the maximum service load that a RC beam is expected to carry in its life span. The goal is to avoid any potential damage of the tested beam as a result of preloading and dynamical loading since the dynamic signature tests are non-destructive. To this endeavor, the preload (P_{pre}) plus the amplified dynamic load $P_0/(2\xi)$ must not exceed the equivalent service load at midspan (P_{ser}). That is:

$$P_{pre} + P_0 \times \frac{1}{2\xi} \le P_{ser} \ . \tag{2.11}$$

The RC beams tested in this study represent the prototype of one strip of a solid deck (Mayo, 1999). The equivalent service load at midspan was estimated to be P_{ser}=9.1 kips.

Figure 2.1 Steel plates as preload

Eq. (2.11) indicates that the maximum preload decreases as the damping ratio ξ decreases. For a consistent estimation, 2% of critical damping is used and P_0=92.89 lb as determined in Section 2.2. Therefore, the maximum preload before inducing additional cracking in concrete is computed as:

$P_{pre}=P_{ser}-P_0/(2\xi)$=(9100-92.89)/(2*0.02)=6778.0 lb. For the beam tests in this project, a maximum preload of 2680 lb was used. This preload represents about 50% of the weight of one beam. During the tests, the preload was simulated by steel plates mounted on the beam near the center point at both sides of the shaker as shown in Fig. 2.1.

2.4. IDENTIFICATION OF FREQUENCY AND DAMPING

The natural frequency and damping of a RC beam can be identified from a transfer function of deflection or acceleration at one point of the beam. The transfer function is a plot of the peak response as a function of the excitation frequency of harmonic loads as schematically shown in Fig. 2.2. The particular excitation frequency corresponding to the largest peak response is the natural frequency of the beam (Lyon, 1995, James, 1994).

The damping ratio can be determined with the quality factor method (James, 1994) or the half power method. As presented in Fig. 2.2, the maximum peak response (ratio) is defined as:

$$Q = \frac{1}{2\xi} \tag{2.12}$$

from which the damping ratio can be estimated. In the halfpower method, two frequencies corresponding to 50% of the maximum power or 70.7% of the maximum response are located on the transfer function. They are designated as f_1 and f_2 in Fig. 2. 2. The damping ratio can then be determined by:

$$\xi = \frac{f_2 - f_1}{f_2 + f_1}. \tag{2.13}$$

It is noted that the transfer function of a linear system is symmetric about the resonant frequency in the domain around the maximum function.

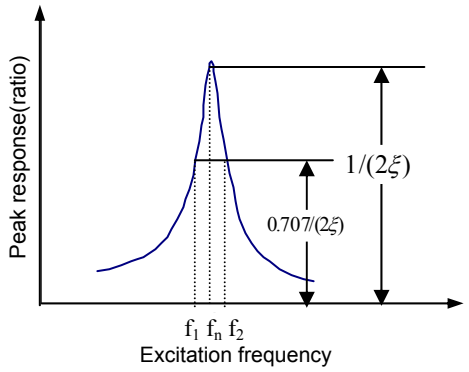

Figure 2.2 Transfer function

3. SPECIMENS, SETUP AND PROCEDURE OF LABORATORY TESTS

3.1. TEST SPECIMEN

Three identical RC beams were cast and tested in the lab. They are 20 ft long, and have a cross section of 15 in wide and 18.5 in deep. The concrete material used has a compressive strength of $f_c^{'}$=5770 psi and an ultimate strain of ε_{cu} = 0.0038 in/in. The concrete beams are reinforced with four steel rebars, 2 No. 5 and 2 No. 6, which are shown in Figure 3.1. A yield strength of f_y =50,000 psi (No. 5) and f_y =80,000 psi (No. 6) is specified (Mayo, 1999). No compression reinforcement was used in the beams and each beam is designed to fail in a ductile manner. The modulus of elasticity of reinforcement is $E_s = 2.9\text{x}10^7$ psi.

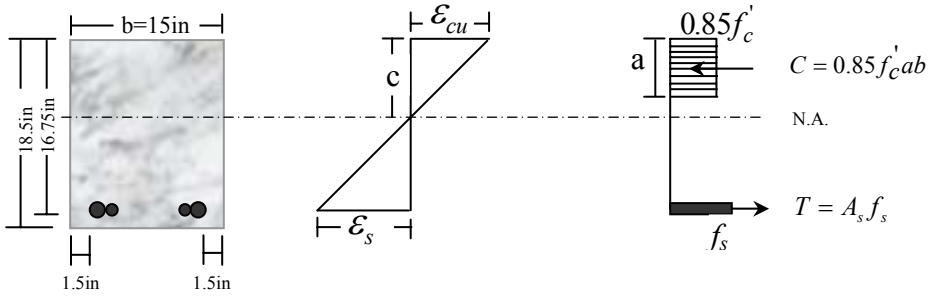

(a) cross section (b) strain (c) forces

Figure 3.1 Beam cross section

The ultimate moment strength of the beam section shown in Figure 3.1 was evaluated using the equivalent rectangular stress block based on the actual ultimate strain of concrete. It was determined to be M_u=130.0 kip-ft. The cracking moment of the section was calculated based on the concrete modulus of rupture $f_r = 7.5\sqrt{f_c^{'}}$ and was found to be M_{cr}=39.31 kip-ft.

3.2. TEST SETUP

Each concrete beam rested on two rollers of 19.0 ft apart. The rollers were supported on two transverse beams that were further anchored into the strong floor. To maintain stability in the transverse direction, four brackets were used at two ends of the beam to prevent any lateral movement during tests. The concrete beam was also tied down to the strong floor at both ends to eliminate potential uplift from its supports as seen in Figure 3.2.

For both static and dynamic tests, a concentrated force was applied at midspan. The static load was provided by a 30-ton hydraulic jack that, in series connection with a 30-ton donut load cell, was installed between a reaction frame and the concrete beam as shown in Figure 3.3. After each static test the load cell was removed to make space for the installation of a shaker. The dynamic load was generated by the shaker. The shaker

was connected to an electric motor by a shaft as shown in Figure 3.4. The operating speed of the motor was controlled by a speed-master device called a control panel.

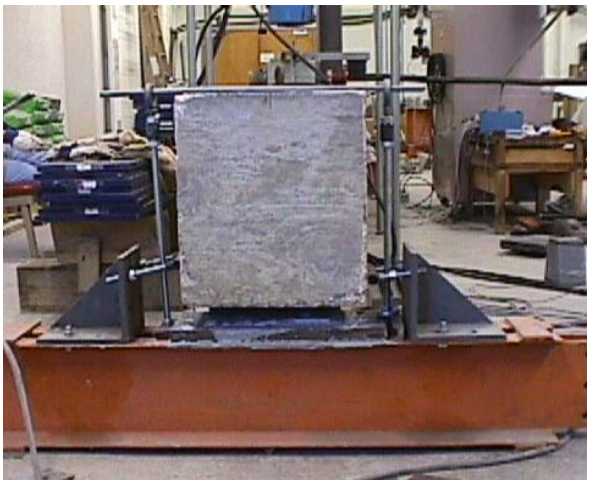

Figure 3.2 Anchor system of beam

The vertical deflections of the beam were acquired at midspan and a quarter point by means of two LVDTs, while accelerations at the same locations were collected using two PCB seismic accelerometers. Four additional LVDTs were placed on the tension and compression side of the beam at midspan and a quarter point so that the curvature could be determined from the collected data. All LVDTs and accelerometers are deployed as illustrated in Figure 3.5.

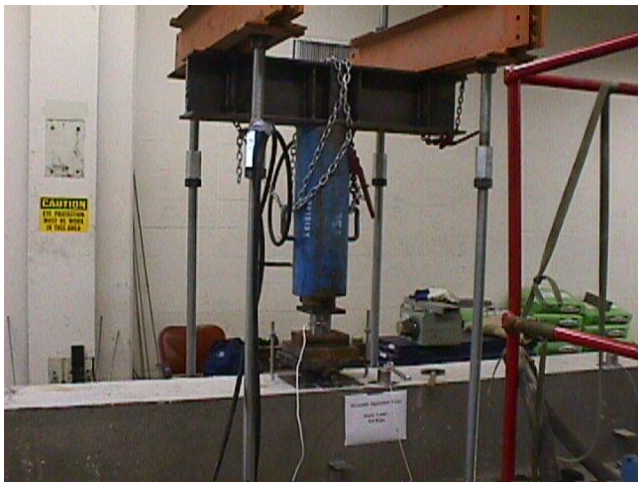

Figure 3.3 Static test setup

Figure 3.4 Dynamic test setup

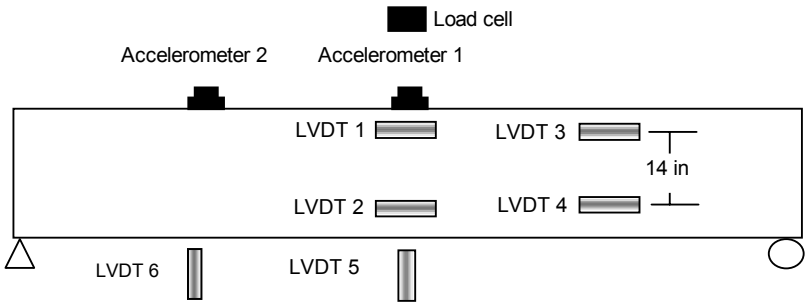

Figure 3.5 Location of transducers

3.3 SURFACE PREPARATION AND INSTALLATION OF CFRP SHEETS

In this study, Beam 3 is strengthened with externally bonded Carbon Fiber Reinforced Polymer (CFRP) sheets (Mayo, 1999). Mbrace CF130 high tensile carbon tow sheets are used here (Mbrace, 1998). They are 0.0065 in. thick per ply and have a design strength of 550 ksi, a design strain of 0.017 in/in and a design tensile modulus of elasticity of 33,000 ksi. Before the installation of CFRP sheets, the beam surface must be prepared according to the recommendations made by the manufacturer. The bottom surface of Beam 3 was sandblasted to remove the laittance at the finishing surface of concrete. The machine used for sandblasting the beam has a capacity of more than 2500 liter/min and a 250-pound sand pot. It was operated under an air pressure of 100 psi. The beam was sandblasted approximately 0.06 in deep until the aggregates of the concrete were exposed. Then the surface was cleaned thoroughly with pressure air for installation of CFRP sheets.

A CFRP strengthening system consists of at least four components, namely primer, putty, CFRP sheets and saturant as shown in Figure 3.6. A thin layer of primer was applied to the bottom surface of the beam with a roller and was then cured. The primer is used to fill the microscopic holes in the concrete.

Next, the putty was applied on the top of the primer using a trowel. The putty was used to fill the large holes in the concrete and make the surface level enough for placing CFRP sheets. It is not necessary to apply the putty before the primer is completely dry.

Because the bottom surface of the beam was relatively smooth and level, only a very thin layer of putty was applied.

When the putty was dry enough, the first layer of saturant (resin) was applied on the surface. After about 20 minutes, the first carbon tow sheet was applied on the resin layer and another layer of resin was applied on the sheet. A plastic roller was used to remove the air trapped under the sheet. This procedure also helps to ensure the CFRP sheet is saturated in the resin. After another 30 minutes, the second layer of resin was applied on the surface and the above installation procedures were repeated to apply the second layer of CFRP sheets.

For Beam 3, two 19 feet long and 10 inches wide plies of Mbrace CF130 tow sheets were used. The above procedure was followed to apply the CFRP sheets. The beam was left to be cured for at least one week before being tested. After strengthening with two plies of CFRP sheets, the strength was expected to increase by 40-50%.

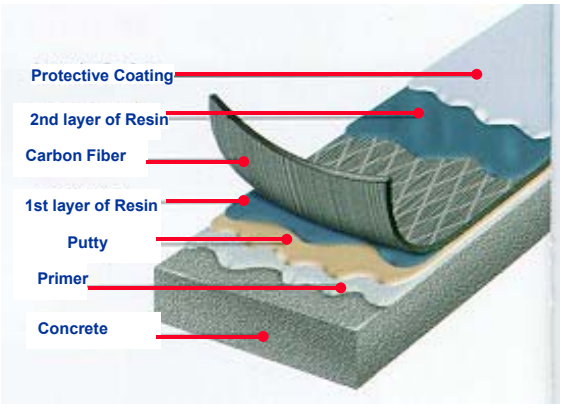

Figure 3.6 CFRP strengthening system

3.4 TEST PROCEDURE

Each concrete beam was tested to failure statically in seven stages. For each stage, the beam was gradually loaded at midspan to 8, 10, 14, 18, 22, or 26 kips, respectively. After that, the beam was continuously loaded to failure. A series of dynamic tests were conducted on the beam in its virgin state and between two consecutive static tests. For each cycle of static and dynamic test, two steps were included:

Step 1: Statically load and unload the beam at midspan to a predetermined load level. Two runs were made to ensure the repeatability of the data.

Step 2: Dynamically test the beam with a sine or a swept-sine load at midspan.

Steel plates were used as preload before the dynamic tests on Beam 1 and Beam 2. The preload for Beam 1 was respectively 2*300 lb, 2*560 lb, 2*820 lb, 2*1080 lb, and 2*1340 lb. The preload for Beam 2 was 2*1080 lb only. For the harmonic tests, a range of excitation frequencies were selected. Each run was carried out with one frequency and the dynamic tests were completed with loads of either increasing or decreasing frequencies in sequence. For the swept-sine test, a single dynamic load with increasing and then decreasing frequency was applied on the beam.

4. TEST RESULTS AND ANALYSIS

4.1 STATIC TESTS

Three RC beams were tested to failure using a single concentrated load at midspan of the beams. For Beams 1 and 2, the static load was applied cyclically twice at each load level. For Beam 3, strengthened with externally-bonded CFRP sheets, the static test was completed with one loading and unloading cycle only. The load versus midspan deflection curves of all three beams are respectively plotted in Figure 4.1-Figure 4.3.

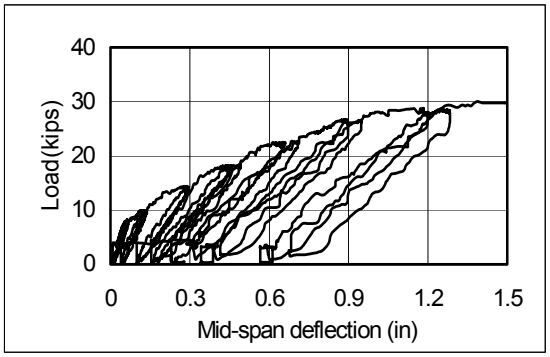

Figure 4.1 Load versus midspan deflection of Beam 1

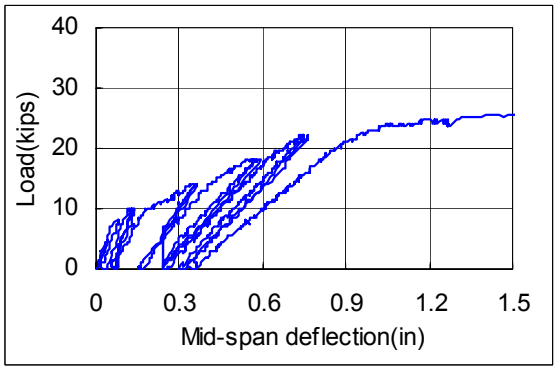

Figure 4.2 Load versus midspan deflection of Beam 2

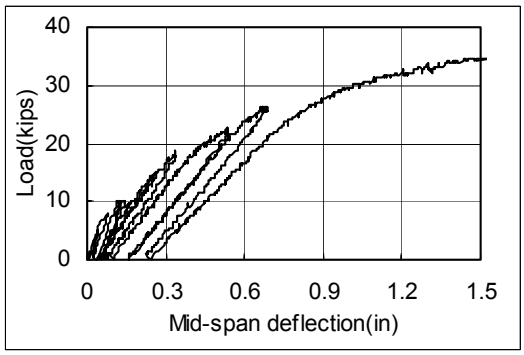

Figure 4.3 Load versus midspan deflection of Beam 3

It is observed from Figs. 4.1 and 4.2 that crack initiates at a load of about 8 kips for Beams 1 and 2. The maximum moment of the beams at this load level is equal to 38 kip-ft, which agrees well with the theoretical analysis. The first beam collapses at about 30 kips while the second at about 26 kips. This corresponds to an ultimate moment of 142.5 kip-ft and 123.5 kip-ft, respectively. Both are close to the theoretical prediction M_u=130 kip-ft. Due to the strengthening of CFRP sheets, the third beam cracks at 18.0 kips and fails in concrete crushing and peeling of the CFRP sheets at 34 kips. Both loads agree with the theoretical results. Unlike the first two beams, Beam 3 does not appear to have a strength plateau after yielding of rebars due to the elastic behavior of CFRP sheets. Overall, all beams behave nonlinearly due to cracking of concrete and yielding of reinforcement.

It is of interest to know whether the beam stiffness degrades significantly. Figs. 4.1 and 4.2 indicate that the stiffness degradation is unlikely to have taken place. A closer look on this issue is made by studying the two cycles of static tests of Beam 1 at the same load level as shown in Figure 4.4. It can be clearly seen that the slope of the load deflection curves has little difference between two consecutive cycles of tests. This confirms the early observations from the entire load-deflection curves.

Although the dynamic load used in the tests is much smaller in magnitude than the static load, it may change the response of a cracked beam. Therefore, upon the completion of dynamic tests at the 6th stage, one cycle of static test up to the load at the previous stage was repeated for Beam 1. Figure 4.5 shows the load deflection curves of Beam 1 at the load level of 26.0 kips. Obviously, the slope of the load deflection curves remains the same before and after the dynamic tests, indicating little effect on the stiffness. The load deflection curve appears to have shifted to the right side of larger deflections. It was concluded that the deflection shift results from the uncorrelated recording of deflections before and after the dynamic tests. However, the area of the hysteresis loop is appreciably reduced due to the shaking in dynamic tests. This implies that the crack surface condition have been changed so that a significant portion of the energy dissipated by the internal friction force is lost.

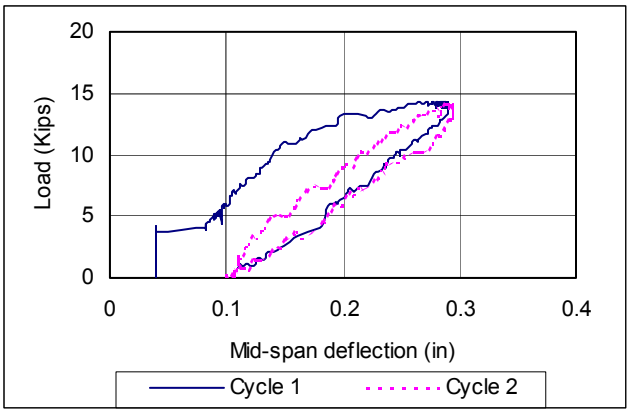

Figure 4.4 Stiffness degradation of Beam 1 (P_s=14 kips)

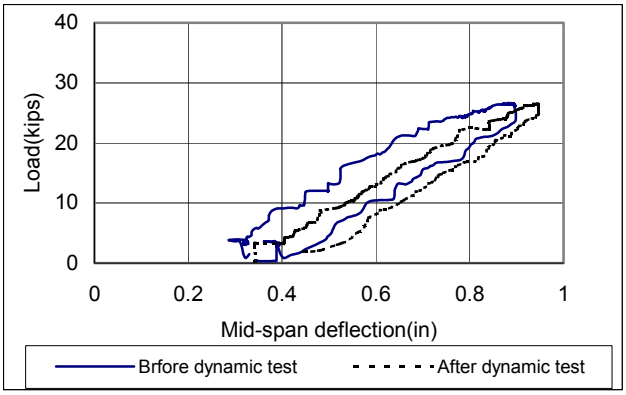

Figure 4.5 Dynamic effect on beam responses (P_s=26 kips)

4.2 DYNAMIC TESTS

The first RC beam was tested in November of 1998 as a pilot study for the entire project. Although the dynamic test on Beam 1 was not extensive, some interesting points such as the preload effect, unstable vibration, and the load-history effect were observed. After the test, a more detailed plan for the test of Beams 2 and 3 was executed to confirm the findings from the first beam tests and to explore new indicators for the detection of damage. The second and third beams were tested in August of 1999. A complete set of the deflection transfer functions are attached in Appendix A, B, and C for Beam 1, Beam 2 and Beam 3 respectively.

4.2.1 Fundamental Frequency of Beams

The fundamental frequencies of the beams or beams plus preload are identified from transfer functions as discussed in Section 2.4. A displacement or acceleration transfer function of a RC beam is determined by testing the beam a dozen of times under harmonic loads, each corresponding to one excitation frequency. Tables 4.1 to 4.3 list the fundamental frequencies of all three beams for different load cases. As one can see, the fundamental frequency of Beams 1 and 2 decreases significantly as the level of static load increases. However, the frequency of the third beam, strengthened with externally-bonded CFRP sheets, drops considerably at the initiation of cracking and then remains nearly constant due to the existence of CFRP sheets. It is also observed from these tables that the fundamental frequency decreases as the preload goes up.

The fundamental frequency of the beams can also be determined analytically by Eq. 2.1. Due to various degree of cracking, the effective moment of inertia changes along the span length. At a particular section, the effective moment of inertia also decreases as the static load increases. The effective moment of inertia is used to represent the overall property of the beams. It can be estimated by (ACI 318-99):

$$I_e = \left(\frac{M_{cr}}{M_a}\right)^3 I_g + \left[1 - \left(\frac{M_{cr}}{M_a}\right)^3\right] I_{cr} \tag{4.1}$$

Table 4.1 Fundamental Frequency of Beam 1

Prelaod	Static load P_s (Kips)						
W_p (lb)	0	8.0	10.0	14.0	18.0	22.0	26.0
0	22.50	22.00	19.35	16.60	15.40	14.50	14.00
2*300	21.00	-	-	-	-	-	-
2*560	19.50	-	-	-	-	12.20	-
2*820	17.75	17.10	15.00	12.80	11.80	11.00	10.80
2*1080	16.45	-	-	-	-	-	-
2*1340	15.25	14.80	13.30	11.30	10.20	9.80	9.70

Table 4.2 Fundamental Frequency of Beam 2

Prelaod	Static load P_s (Kips)					
W_p (lb)	0	8.0	10.0	14.0	18.0	22.0
0	21.75	21.25	19.75	18.25	17.25	-
2*1080	15.60	15.25	14.25	12.00	-	-

Table 4.3 Fundamental Frequency of Beam 3

Prelaod	Static load P_s (Kips)					
W_p (lb)	0	10.0	14.0	18.0	22.0	26.0
0	23.00	19.75	18.25	18.25	18.75	18.50

where M_{cr} and M_a respectively denote the cracking moment and the applied bending moment, I_{cr} and I_g represent the moment of inertia of the transferred cracked section and the uncracked gross section,respectively. In Eq. (4.1), the cracking moment is calculated by:

$$M_{cr} = \frac{f_r I_g}{h/2} \tag{4.2}$$

in which f_r is the modulus of rupture, equal to $7.5\sqrt{f_c'}$ and h represents the overall height of a beam section. Wang *et al* (Wang, 1998) modified the above formula for I_e into:

$$I_e = \left(\frac{M_{cr}}{M_a}\right) I_g + \left[1 - \left(\frac{M_{cr}}{M_a}\right)\right] \alpha I_{cr} \tag{4.3}$$

where α is a constant varying from 1.05 to 1.15 for a cracked beam section subjected to the applied bending moment and from 1.35 to 1.5 for a cracked beam section without load. These results are based on the limited test data on simply-supported beams and may need further investigation for other support conditions, reinforcement ratio, concrete strength and size effect.

For Beams 1 and 2 whose cross-section is sketched in Figure 3.1, the moments of inertia of the uncracked and cracked sections are respectively equal to I_g=7915 in^4 and I_{cr}=1929 in^4.

The equivalent moment of inertia calculated from Eqs. (4.1) and (4.3) and the fundamental frequencies of Beams 1 and 2 determined by Eq. (2.1) are listed in Table 4.4. The applied moment M_a is the maximum moment at the stage for which the deflection and effective moment of inertia are calculated. To visualize how the natural frequency varies with the static load, the fundamental frequencies are normalized by that of the virgin beams and plotted as a function of the ratio of the static load and the ultimate load as shown in Figure 4.6. It is observed that the Wang's equation of (4.3) leads to the analytical frequencies that are in excellent agreement with the test data of Beam 2 and change with static loads in the same trend as the experimental results of Beam 1 indicate. However, the ACI equation of (4.1) significantly underestimates the fundamental frequency. This is because the ACI equation is developed for the deflection control of beams and thus renders a conservative design. Therefore, for the purpose of studying the behavior of concrete beams, it is not advisable to use the ACI equation.

Table 4.4 Measured and Predicted Frequency of Beams

Static load (kips)	0	8.0	10.0	14.0	18.0	22.0	26.0	28.0	Note
M_a(k-ft)	0	38.2	47.75	66.85	85.95	105.05	124.15	133.70	
I_e(in^4)	7915	7915	5287	3146	2501	2242	2119	2081	Eq. 4.1
f(Hz)	22.34	22.34	18.23	14.08	12.56	11.89	11.56	11.45	
I_e(in^4)	7915	7915	6976	5727	5033	4591	4285	4165	Eq. 4.3 with α=1.35
f(Hz)	22.34	22.34	20.97	19.00	17.81	17.01	16.44	16.21	
Ie(in^4)	7915	7915	7027	5846	5190	6772	4483	4370	Eq. 4.3 with α=1.5
f(Hz)	22.34	22.34	21.05	19.20	18.09	17.35	16.81	17.00	
f of Beam 1	22.50	22.00	19.35	16.60	15.40	14.50	14.00	-	Measured
f of Beam 2	21.75	21.25	19.75	18.25	17.25	-	-	-	Measured

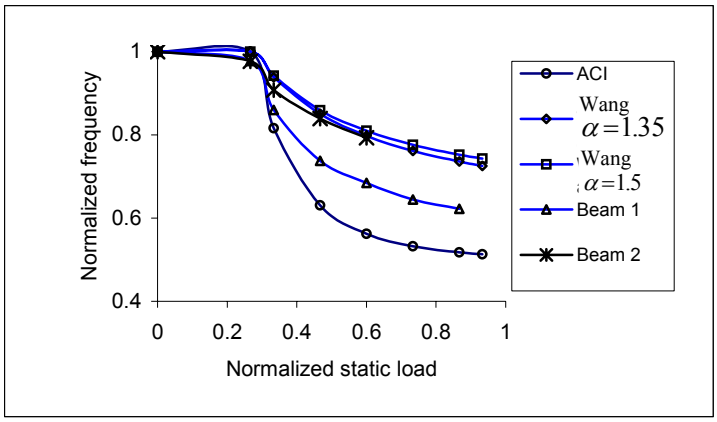

Figure 4.6 Frequency variation with damage states

The fundamental frequencies identified from the laboratory test of all three beams are presented in Figure 4.7. It can be seen that Beams 1 and 2 are continuously subject to substantial reduction in stiffness and frequency from initial cracking to collapse of the beams. The frequency of Beam 3 seems to remain constant after the stage for which the static load was 14.0 kips. This is because the external CFRP sheets bonded at the tension

surface of Beam 3 will take over a substantial part of the tensile stress after this stage. Therefore, the stiffness and frequency of Beam 3 do not change too much after that stage due to the elastic property of CFRP sheets up to failure. Indeed, it was observed during the test that after the initial cracking in concrete, cracks extended slowly with increasing static load. Until the last stage when the beam was loaded to a complete failure, sizable cracks extended quickly, causing concrete crushing and the peeling of CFRP sheets.

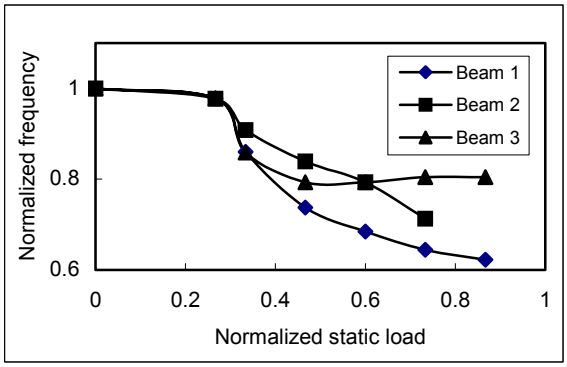

Figure 4.7 Fundamental frequency of beams

4.2.2 Effect of Preload on Dynamic Signatures

The effect of preload on the fundamental frequency of a beam can be determined from Eq. (2.3). The fundamental frequency of Beam 1 or 2 plus a preload is normalized by that of the beam alone and the ratio is shown in Figure 4.8. It is noted that P_s/P_u in Figure 4.8 represents the ratio of the static load on a beam and the ultimate load of the beam from tests.

As indicated in Tables 4.1 and 4.2, Beams 1 and 2 are subject to severe cracking and possible yielding of reinforcement when a static load over 10 kips is applied. Both beams behave inelastically. Figure 4.8(c) also shows that the frequencies calculated by Eq. (2.3) agree well with the experimental results. Although both Eq. (2.1) and Eq. (2.3) are derived for elastic structures, their frequency ratio captures the characteristics of inelastic structures as well. It can also be observed from Figure 4.8 that the preload effect on frequency is independent of the level of load that a beam ever carries. Therefore, the analytical prediction by Eq. (2.3) is applicable to all cases. This is because the dynamic responses of the beams are smaller in magnitude than that induced by the static load. Such responses are not sufficient enough to completely close the visible cracks in the beams. Therefore, the occurrence of pounding between two sides of such cracks was not indicated by reviewing the response time histories throughout the tests. However, it was found that preloading does significantly affect the amplitude and "resonance" frequency of the beams as evidenced from the transfer function shown in Figure 4.9. It is indicated from the figure that when a static load of 81% or 96% of the ultimate load was applied on and then removed from Beam 1, the maximum dynamic responses of the beam without preload appreciably differ from each other and occur at different excitation frequencies if the beam is excited from low-to-high and high-to-low frequency, respectively. However, both the peak response difference and frequency shift are significantly suppressed as soon as a preload of 30% of the beam weight is applied on the beam as indicated in Figure 4.9(b). The time history of the beam response thus becomes stable as shown in Figure

4.10. This is probably because the preload can keep the micro-cracking at the tip of visible cracks open. The micro cracking is believed to contribute to the frequency shift and change in the corresponding peak response. Further discussions on this phenomenon are provided in Section 4.2.4.

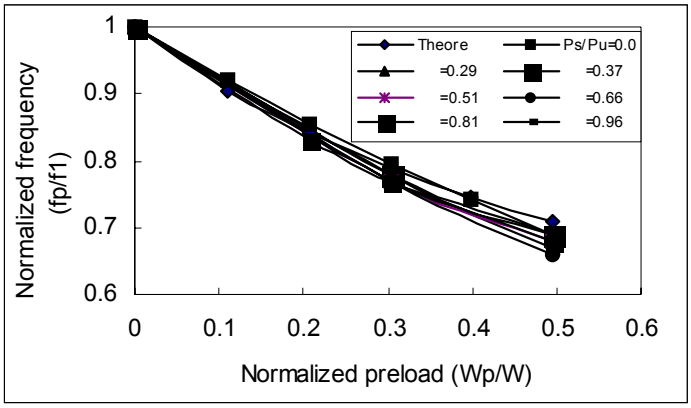

(a) Beam 1

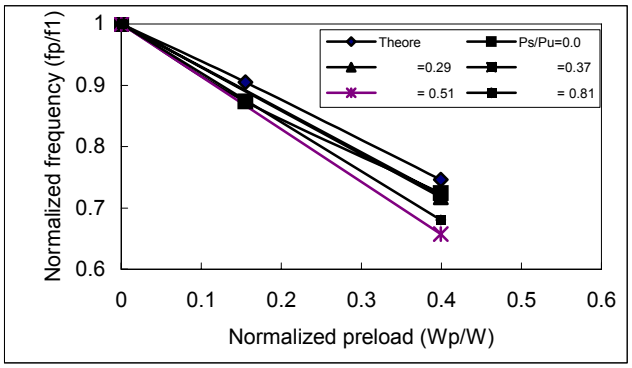

(b) Beam 2

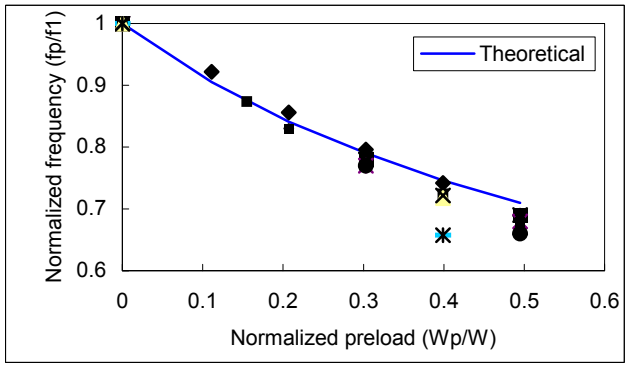

(c) Beam 1 and Beam 2

Figure 4.8 Preload effect on natural frequency

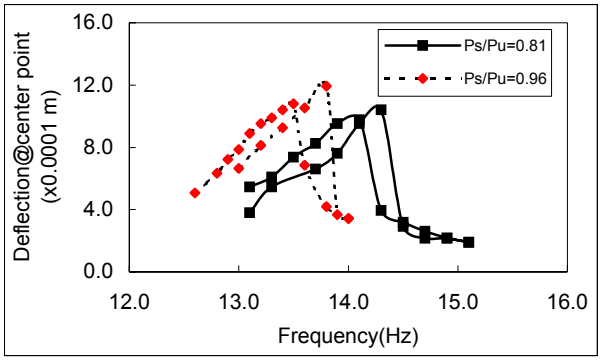

(a) $W_p/W=0.0$

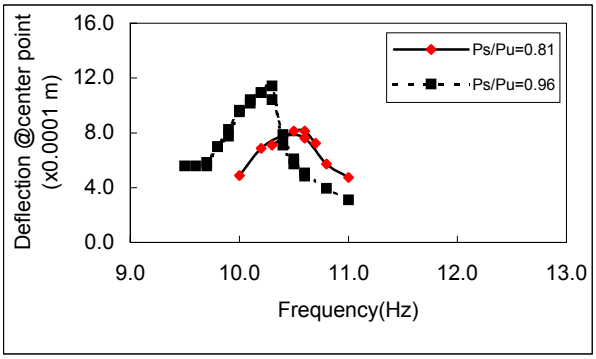

(b) $W_p/Wbeam=0.3$

Figure 4.9 Preload effect on transfer function

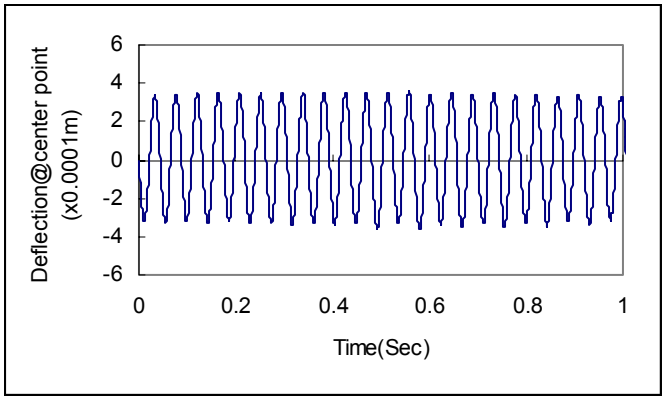

Figure 4.10 Time history response of beam

4.2.3 Damping Ratio of Beams

Using the half-power method discussed in Section 2.4, the damping ratios of Beams 2 and 3 are respectively listed in Tables 4.5 and 4.6 when preload is not present. As implied in Figure 4.9, the damping ratios are loading history dependent and take different values when the beam is tested under harmonic loads in the order of increasing or decreasing excitation frequencies. They are presented separately in Figs. 4.11 and 4.12. The damping ratio of a beam tested with excitation frequency increasing is always smaller than that with excitation frequency decreasing. Surprisingly, the damping ratio of

both beams, when tested with increasing frequencies, only changes slightly as the static load increases. On the other hand, when tested with decreasing frequencies, damping ratios generally increase with the static load and those of the CFRP-strengthened beam change less than those of the unstrengthened beam.

Table 4.5 Damping Ratio of Beam 2

Static load (kips)	0	8.0	10.0	14.0	18.0	22.0
ζ (%) with increasing Ω	1.8	1.2	1.3	2.0	1.9	1.9
ζ (%) with decreasing Ω	1.8	1.4	1.5	3.2	3.1	3.7

Table 4.6 Damping Ratio of Beam 3

Static load(kips)	0	10.0	14.0	18.0	22.0	26.0
ζ (%) with increasing Ω	1.8	1.2	1.3	1.4	1.4	1.8
ζ (%) with decreasing Ω	1.8	2.2	2.0	2.3	3.0	3.1

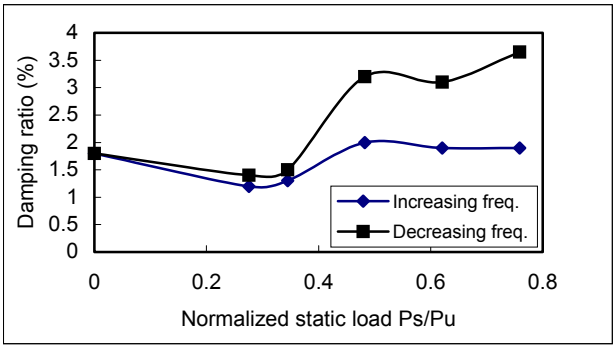

Figure 4.11 Damping ratio of Beam 2 with the severity of damage

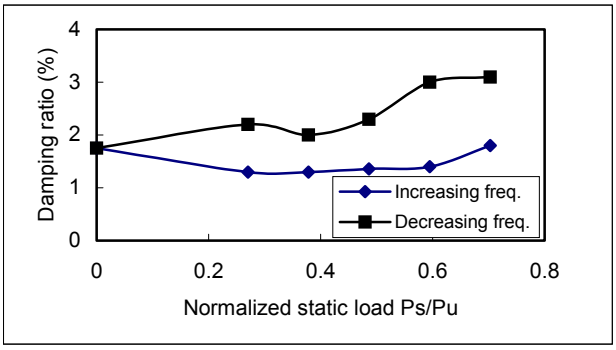

Figure 4.12 Damping ratio of Beam 3 with the severity of damage

4.2.4 Loading History Dependence of Dynamic Signatures

It was observed during the test of Beam 1 that the beam vibrated in a constant amplitude for a short while and then suddenly dropped to a much smaller amplitude at certain range of excitation frequencies. Figure 4.9(a) also indicates that the transfer functions of the beam significantly change with the testing sequence—increasing vs. decreasing frequencies. In addition, these transfer functions are not symmetric about the "resonant" frequency in the domain of the peak response. The jumping phenomenon, load history dependence and unsymmetric transfer functions are characteristics of the nonlinear vibration. The beam therefore experienced nonlinear vibration after severe cracking.

Similar observations can be made from the tests of Beams 2 and 3 as shown in Figure 4.13. It can be seen that the transfer functions are skewed in the domain of the peak response to the low frequency side. The skewness of the transfer function decreases as the number of test increases, implying the transient feature of a newly-damaged beam. The frequencies corresponding to the peaks of different transfer functions vary significantly, indicating the dependence of the resonant frequency on the loading history. While the above phenomena represent the typical nonlinear vibration problem of a softening system, these characteristic frequencies eventually converge to a resonant frequency after the beam is tested in about 30 minutes. This may be attributable to the presence of micro cracks whose surface condition is time dependent but soon stabilized after a significant number of cycles of vibration tests. The beam then vibrates elastically as the final transfer function indicates. This phenomenon exists in both unstrengthened and CFRP strengthened beams.

The above discussion indicates that the shift of the characteristic frequency, corresponding to the maximum transfer function value, is closely related to the new damage in a beam. Therefore, the frequency shift could be an effective damage indicator that is particularly useful in evaluating damage in RC structures immediately after the damage occurs. Unlike the natural frequency discussed in Section 4.2.1, the frequency shift does not depend on the accumulative damage in a RC structure over its service life and could have a potential impact on the development of no-baseline damage detection techniques.

The frequency shift of Beams 2 and 3 without preload are respectively normalized by their corresponding natural frequencies of elastic beams. They are listed in Table 4.7 and depicted in Figure 4.14. As one can see, the frequency shift increases with the static load for both unstrengthened and strengthened RC beams. More importantly, the rate of frequency shift is much higher when P_s/P_u exceeds 0.4~0.5 or when the beam is subjected to a service load (P_{ser}/P_u=0.35 for Beam 2) or slightly higher. In addition, the normalized frequency shift presented in Figure 4.14 involves the subtraction and division of the three "resonant" frequencies measured in an identical testing environment using the same equipment and data acquisition. Both systematic and random errors in the determination of the normalized frequency shift are expected to be much smaller than those of the

natural frequency discussed in Section 4.2.1. Therefore, it is reasonable to conclude that damage occurs in a beam when $\Delta f/f_1$ is greater than (2~3)%.

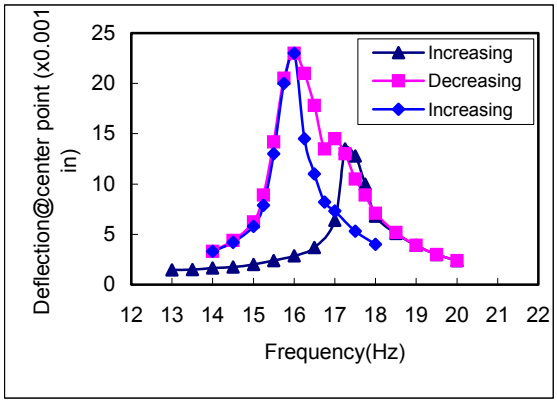

(a) Beam 2 (P_s=18 kips)

(b)

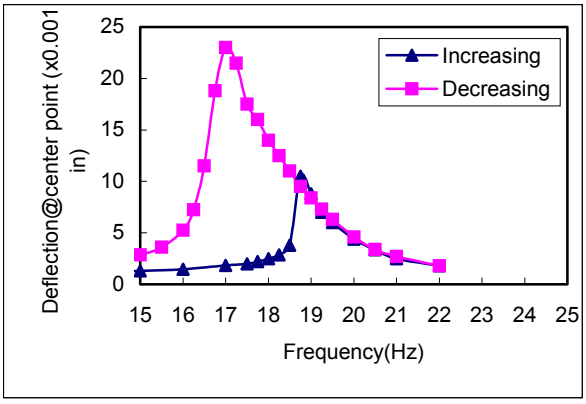

(c) Beam 3 (P_s=22 kips)

Figure 4.13 Loading history dependence of resonant frequency

Table 4.7 Frequency Shift vs. Static Load

Beam 2: RC beam						
Static load P_s (kips)	0	8	10	14	18	22
Normalized static load P_s/P_u	0.0	0.31	0.39	0.54	0.70	0.85
Frequency shift Δf (Hz)	0.0	0.25	0.25	0.75	1.25	2.25
Normalized frequency shift $\Delta f/f_1$ (%)	0.0	1.15	1.15	3.45	5.75	10.35
Beam 3: CFRP-strengthened RC beam						
Static load P_s (kips)	0	10	14	18	22	
Normalized static load P_s/P_u	0.0	0.27	0.38	0.49	0.60	
Frequency shift Δf (Hz)	0.25	0.5	0.5	0.75	1.75	
Normalized frequency shift $\Delta f/f_1$ (%)	1.09	2.17	2.17	3.26	7.61	

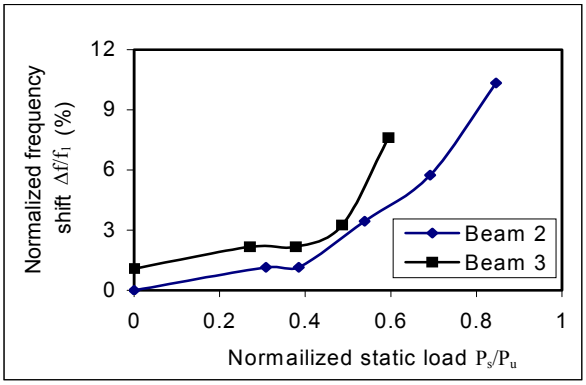

Figure 4.14 Natural frequency shift with the severity of damage

4.2.5 Failure Mode of Beams

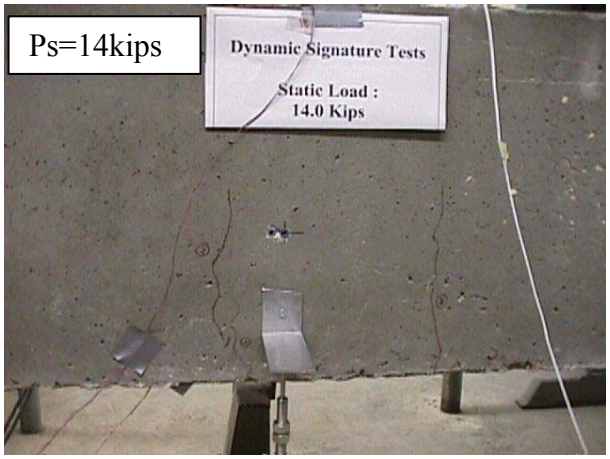

(a) P_s=14kips

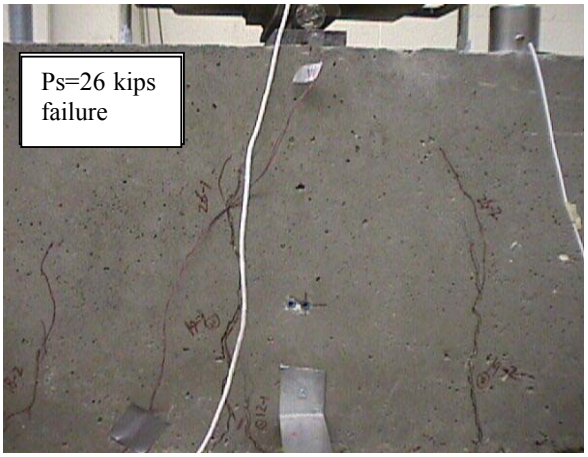

(b) P_s=26kips

Figure 4.15 Cracks in an unstrengthened beam

All three beams are reinforced with two No. 5 and two No. 6 steel rebars, equivalent to a 0.6% steel ratio. They are underreinforced RC members. Beams 1 and 2 are unstrengthened and Beam 3 is strengthened with 2 plies of CFRP sheets. For the first two beams, cracks progressed rapidly until failure after the initiation of cracking as the static load on the beams increased. The first crack appeared at the center of the span when the static load is equal to 10 kips. After that, cracks developed almost symmetrically about midspan. Eventually, excessive deflections were observed and the test was terminated. Figure 4.15 shows the flexural crack patterns near midspan corresponding to two static loads. For the CFRP strengthened beam, cracks developed in a similar pattern at the early stage since CFRP sheets contribute little to the cracking moment at this stage. However, the cracks of the CFRP strengthened beam were almost completely closed until P_s reached 22 kips, while those in the unstrengthened beams were not after 14 kips of static load. As the static load continued to increase, the cracks extended further so that the compression zone became smaller and smaller. In the end, failure occurred due to crushing of concrete as evidenced from Figure 4.16. It was also observed that a small strip of CFRP was peeled off as seen in Figure 4.17. After peeling of CFRP sheets, the strengthened beam collapsed.

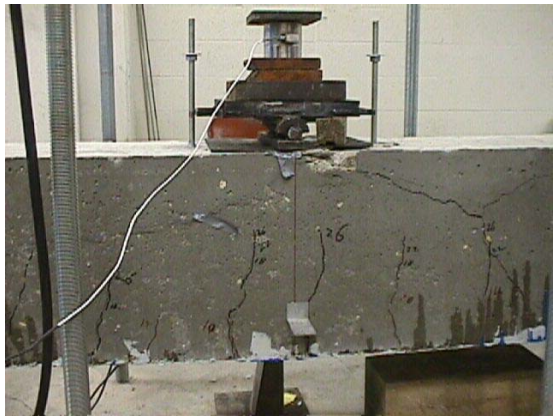

Figure 4.16 Failure of a CFRP strengthened beam

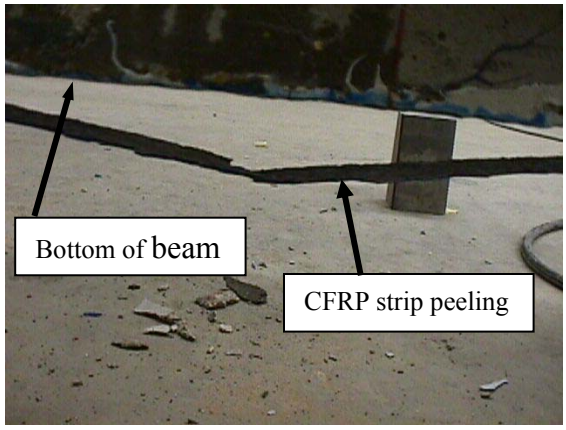

Figure 4.17 Peeling of a CFRP strip

4.3 CONCLUSIONS

Based on the laboratory tests of the three RC beams, the following conclusions can be drawn:

1. The cracking and ultimate moments determined from the test results are in good agreement with those calculated based on the material properties. This agreement indicated that the material properties obtained by the coupon tests are sufficiently accurate.
2. The stiffness degradation due to the cyclic loading at constant amplitude is insignificant. The dynamic test between two consecutive static tests have negligible effect on the stiffness of the beam. However, the dynamic test does notably reduce the hysteretic damping of the cracked RC beams.
3. The effect of an additional weight on the natural frequency of a beam can be analytically evaluated regardless of the severity of damage occurring in the beam. This additional weight can effectively improve the stability of a severely cracked, simply supported beam.
4. The natural frequency corresponding to the peak of a transfer function depends on the loading history. It is typically larger when the transfer function is determined with a series of harmonic tests of increasing excitation frequency in sequence. The associated damping ratio is smaller and changes with the severity of damage less significantly.
5. At any state of damage, the shift in natural frequency becomes smaller as the number of cycles of dynamic test increases. It represents the transient feature of a newly-cracked beam and therefore can be used as an effective indicator in damage detection without knowing the damage history of the beam. The maximum shift in natural frequency correlates very well with the severity of damage in the beam.
6. The CFRP sheets externally-bonded to the tension face of a beam can keep cracks in the beam closed until the sheets are ruptured or pealed off. Consequently, the natural frequency of a CFRP-reinforced beam reduces significantly at the initiation of cracking but remains nearly constant afterwards.

5. DYNAMIC SIGNATURE TESTS OF PROTOTYPE BRIDGE DECKS

5.1 INTRODUCTION

Bridge J857 was located on Highway 72, 11 miles from Rolla, Missouri. The bridge was constructed in 1932 and consisted of three simply supported solid RC decks. Each deck was 26.0 ft long, 26.0 ft wide, 1.5 ft thick and had a skew angle of around 15 degrees with the bridge center line. An overview of the bridge is shown in Figure 5.1.

Figure 5.1 Bridge J857

West span (Rolla side) was reinforced with near-surface FRP rods and Center span was strengthened with externally CFRP sheets. The third span on the east side of the bridge (Salem side) was unstrengthened and used as a benchmark. Since the end of August 1998, a series of destructive and non-destructive tests had been conducted on the bridge decks by the University of Missouri-Rolla and University of Missouri-Columbia researchers in order to validate new strengthening technologies and damage detection techniques, such as externally-bonded CFRP sheets, near surface mounted FRP rods and dynamic signature tests for detecting the overall damage in RC decks. The bridge was demolished in April 1999.

5.2 DYNAMIC TESTS

5.2.1 Purpose and Significance

Dynamic characteristics such as frequency of a structure are directly related to the stiffness and geometry of the structure. Any change in these structural properties will alter the frequency and therefore can be identified based on the observation on dynamic characteristics of the structure. This section is focused on the correlation study between the severity of damage and the change in resonant frequency as well as damping of the bridge decks.

The natural frequency and damping can be extracted from dynamic test data. In this study, a series of forced vibration tests were conducted on Bridge J857. They require a short period of time to set up in the field condition and a minimum interaction with in-service bridges. Essentially, the vibration tests used in this study are non-destructive to structures and can be used to assess the structural conditions of in-service bridges by

detecting the severity of damage in a bridge after an event such as truck collision or earthquake.

5.2.2. Test Procedure and Setup

For the dynamic tests on Bridge J857, a harmonic load was generated by a shaker and applied at midspan along the bridge centerline. Dynamic and static tests were conducted in parallel. The bridge deck was gradually tested to failure in several stages with four hydraulic jacks. A series of dynamic tests were conducted between two consecutive stages of the static tests following the same procedure as used for the beam tests in laboratory. The acceleration responses at various points were acquired corresponding to different exciting frequencies. Obtained from these responses are the transfer functions of the measured parameters, from which the frequency and damping of the bridge can be identified. The changes in frequency and damping represent the variation of overall structural conditions.

At the beginning of 1999, the research team at UMR decided to purchase two (2) data acquisition and twelve accelerometers for the dynamic tests. Unfortunately, they were not available yet at the time of testing on the West and Center spans. Therefore, the first deck (West span) was statically tested to failure without dynamic tests in between. For the middle deck, four accelerometers were deployed along the longitudinal and transverse centerlines as shown in Figure 5.2. Right before the test of the last spans, the data acquisition systems and accelerometers became available to the research team. All accelerometers were deployed on the East span as located in Figure 5.2.

A sinusoidal load was applied at the center point as designated #2 in Figure 5.2 for the centerspan, and at the at the midspan (#7) and the quarter point (#8) for the east span. A range of exciting frequencies were selected to span over the estimated natural frequency of the first mode of the bridge deck. Two sets of data for a transfer function were collected by increasing or decreasing the exciting frequencies. The purpose of doing so was to test the repeatability of data for the linear vibration of undamaged stage and to identify the dependence of "resonant" frequency on the loading history after severe cracking of the deck.

Preloads were applied before some dynamic tests to keep microcracks open. They are represented by twelve steel blocks with a total load of about 14% of the deck weight (one span). A total of five (5) cases for the center span and eleven (11) cases for the east span were considered during the dynamic tests. Each case corresponds to a specified static with or without preloading as defined in Table 5.1 with a prefix C.

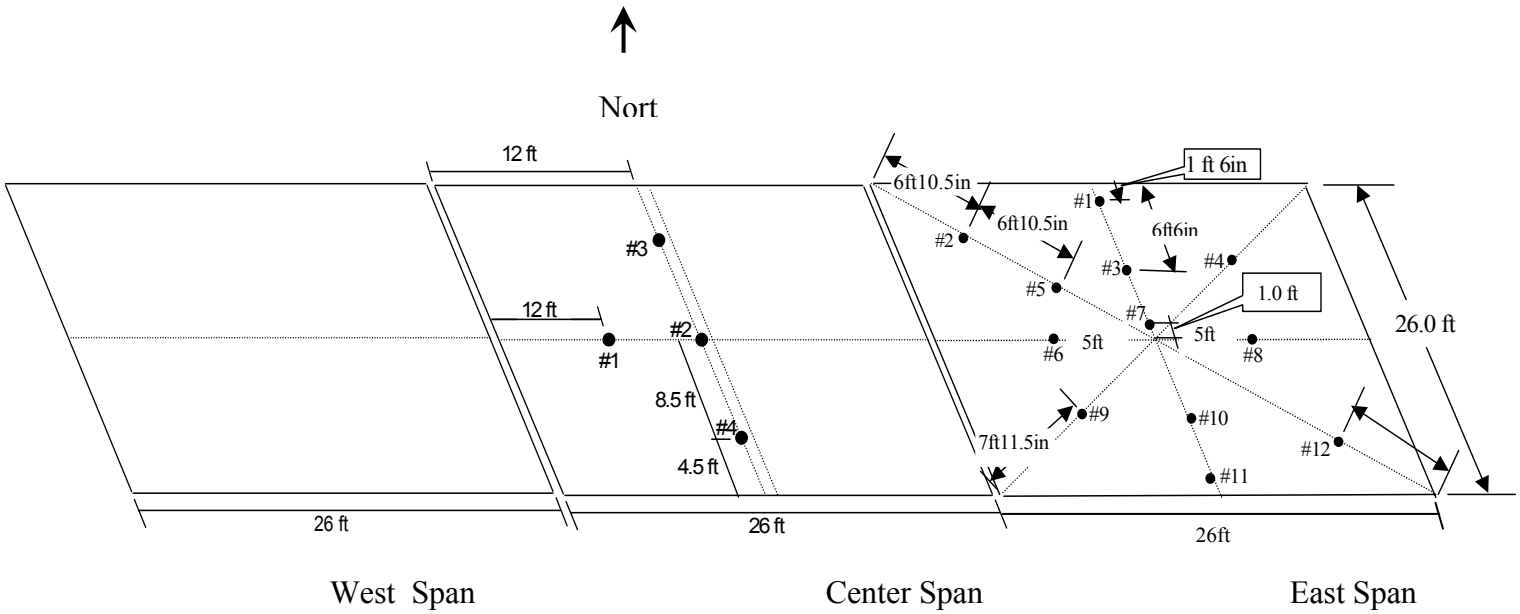

Figure 5.2 Location of accelerometers

Table 5.1 Load Cases of Dynamic Tests

Test Date: 03/16/1999									
Static Load(Kips)		0	100	240	360	480			Center Span
Shaker: Center point	No preload	C1	C2	C3	C4	C5			
Test Date: 02/25/1999									
Static Load(Kips)		0	80	120	180	240	320	464	East Span
Shaker: Center point	No preload	C2	C3	C4	C5	C8	C9	C11	
	Preload				C6	C7			
Shaker: Quarter point	No preload	C1					C10		

The static and dynamic loading systems are shown in Figure 5.3. Twelve steel blocks as preload were moved to the bridge deck by a crane shown in Figure 5.4 and the dynamic responses are recorded with two portable data acquisition systems shown in Figure 5.5.

Figure 5.3 Static and dynamic loading system

Figure 5.4 Preloading before dynamic tests

Figure 5.5 Data acquisition system

5.2.3 Test Results

A complete set of acceleration transfer functions for the center span are attached in Appendix D. Those corresponding to Cases 1, 2 and 5 at the center point (#2) are presented in Figs. 5.6-5.8. In the virgin state, the fundamental frequency is around 16.5 Hz. The second peak on the transfer function corresponding to 17.5 Hz is obtained during all dynamic tests except for the failure loading case (P_s=480.0 kips). A careful examination on the transfer functions of acceleration responses at other points also indicates the existence of the second peak. It is speculated that this frequency may result from nonuniform support at both ends of the deck. When the static load reaches 100.0 kips, the concrete started cracking and the fundamental frequency reduced to 16.0 Hz. However the second frequency basically remained 17.5 Hz. When the deck was loaded to 240 kips and unloaded, the fundamental frequency became slightly less than 16.0 Hz. The change in frequency as the static load increases follows the same trend as observed in Figure 4.7 for Beam 3 strengthened with CFRP sheets. When a static load of 480.0 kips is applied, the CFRP sheets started peeling and the deck cracked significantly along the loading line. It was observed that the fundamental frequency suddenly dropped to 15.0 Hz.

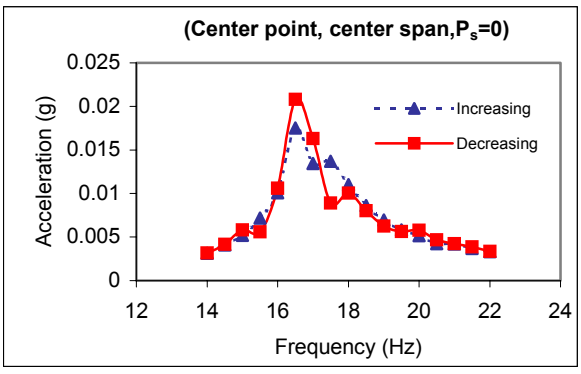

Figure 5.6 Transfer function at virgin state

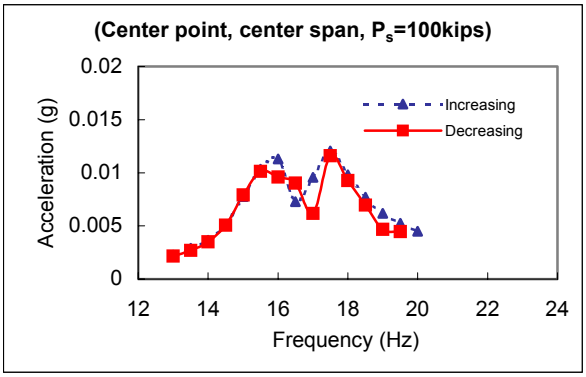

Figure 5.7 Transfer function at cracking state

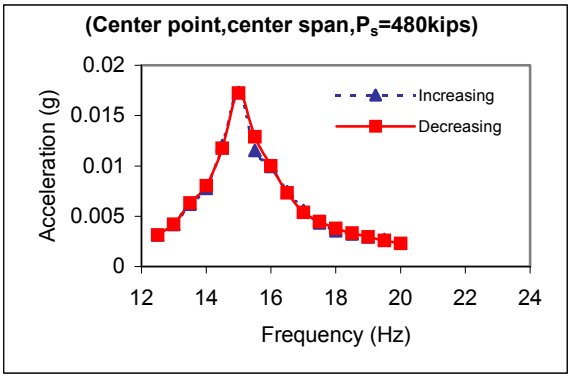

Figure 5.8 Transfer function at failure state

When the harmonic tests are conducted with an excitation frequency increasing or decreasing in sequence, the resonant frequency associated with the fundamental vibration mode slightly shifts as evidenced in Figure 5.8. This observation confirms the findings from the laboratory tests of RC beams as discussed in Section 4.2.4. However, the data collected from the field tests are very limited due to the fact that the bridge has to be demolished on time and is therefore made available for the dynamic tests on the center span for one day only. The sensitivity of the shift in resonant frequency to the severity of damage needs to be further verified in field conditions.

The damping ratio of the fundamental mode is shown in Figure 5.9 as a function of the static load for the center span. It is roughly equal to 3% in the virgin state. As the static load increased, the bridge deck started cracking and therefore damping increased due to the energy dissipation in micro cracks. However, the damping decreased as the deck was close to collapse. This is likely caused by the reduction in percentage of micro-racks as more visible cracks are developed. The overall range of damping ratio is between 3% and 5%. This represents the level of damping of a typical RC structure system.

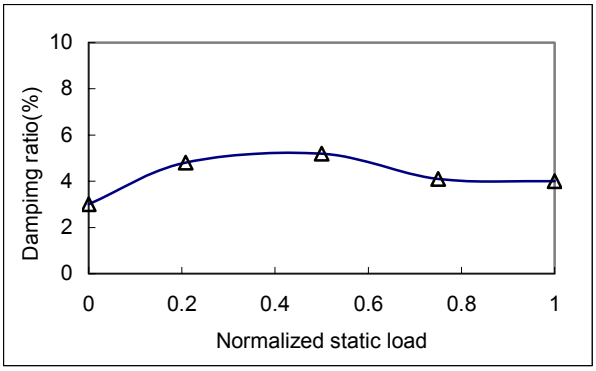

Figure 5.9 Change of damping with static load

More extensive tests had been carried on the east span. Unfortunately, it was found after the completion of the dynamic tests that the test data can not be retrieved due to the improper setup of data acquisition. This occurred because the new equipment was put in use without much chance for the members to practice. Under the pressure of demolishing the bridge on time, the lack of confidence on the equipment resulted in a painful lesson for experimental work.

5.3 FINITE ELEMENT ANALYSIS

The center span was modeled using a commercial software called SAP2000. Natural frequencies and mode shapes of the bridge deck were analyzed using the finite element method. The skew effect was also evaluated using the computer model. The numerical results are compared with the experimental results.

5.3.1 Model Establishment

The geometry of the bridge deck is shown in Figure 5.10. This deck is considered as a thin plate in the computer model as illustrated in Figure 5.11. The model input data are presented in Table 5.2. To simulate the actual boundary conditions, a distributed rotational spring of 300,000 kips-in was added along each edge of AD and BC sides.

5.3.2 Analytical Results

The mode shapes of the first four modes are depicted in Figure 5.12, and the corresponding natural frequencies are listed in Table 5.3. The fundamental frequency is 16.49 Hz, which is in agreement with the experimental result. The skew effect on the fundamental frequency of the deck is shown in Figure 5.13. As the deck becomes more skewed, the frequency increases nonlinearly. For the bridge under investigation, the skew angle is equal to 15^{o}. The skew effect therefore increases the frequency by 7%.

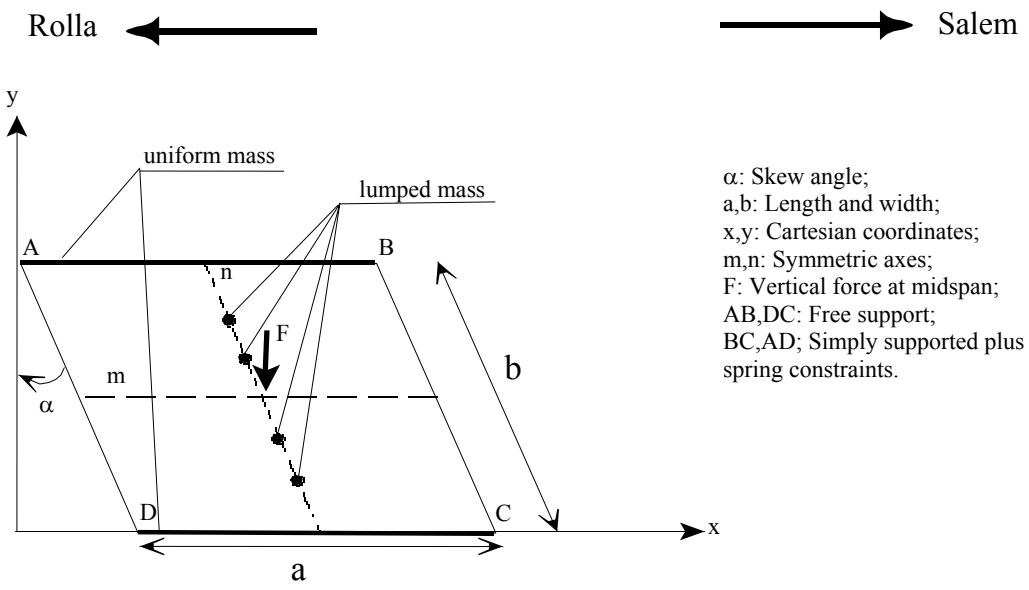

Figure 5.10 Geometry of the deck

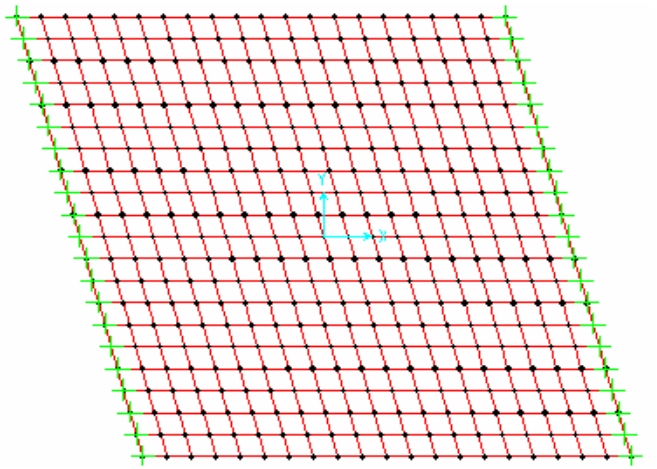

Figure 5.11 Finite element model of Bridge J857

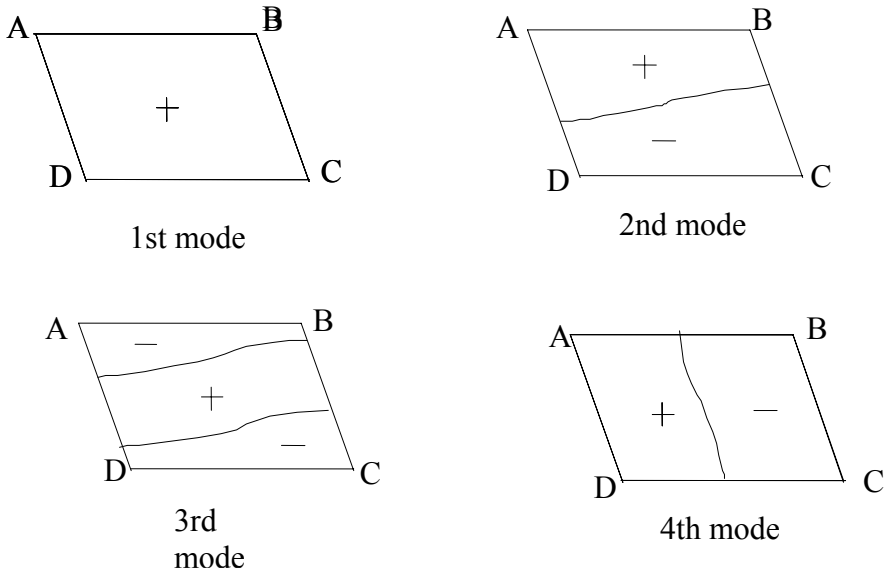

Boundary conditions:
Free support at AB, CD;
Restraints at AD and BC are U1, U2, U3, R1, R3 plus spring $2.5*10^5$ (kip-in) about R2.

Figure 5.12 Mode shapes of the first four modes

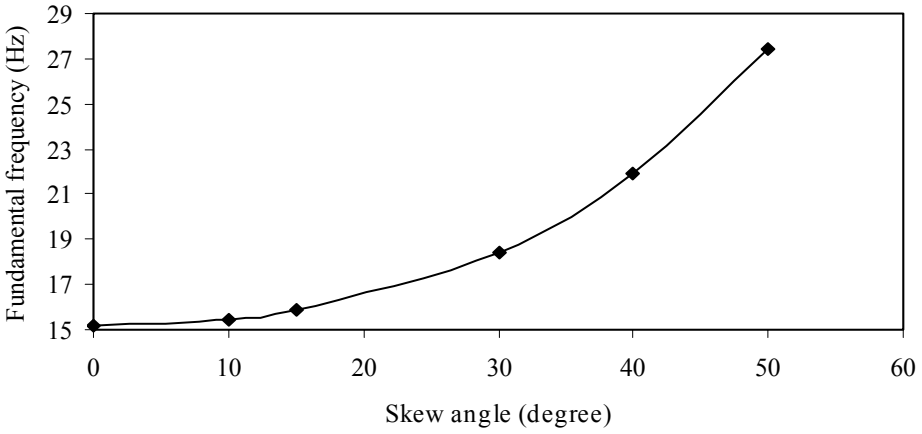

Figure 5.13 Fundamental frequency versus skew angle

Table 5.2 Input Data in Finite Element Model

Deck mass density	Extra mass		Skew angel α	Poisson's ratio	Thickness
	Uniform	Lumped			
$2.248*10^{-4}$ $lb.sec^2/in^4$	0.032 $lb.sec^2/in^2$	1.92 $lb.sec^2/in$	15°	0.2	17.5 in
Boundary condition AB, DC	Boundary condition BC, DA	length a	Width b*sinα	Respect ratio b*sinα/a	Damping
Free	Simply supported plus Spring constraints	26ft	25ft	0.962	3%

Table 5.3 First Four Natural Frequencies of Bridge Deck

1^{st} mode	2^{nd} mode	3^{rd} mode	4^{th} mode
16.49 HZ	22.92 HZ	44.61 HZ	55.72 HZ

Boundary conditions are shown in Figure 5.12.

5.4 CONCLUSIONS

Based on the dynamic tests conducted on Bridge J857 and the model analysis, the following conclusions can be drawn:

1. The shift in fundamental frequency when the bridge was tested with a sinusoidal load of increasing and then decreasing excitation frequency was also observed as for the beam tests in lab. The magnitude of the shift, however, is smaller due to the complexity in the skewed bridge system.
2. The fundamental frequency of a CFRP strengthened deck slightly reduces at the initial cracking of concrete material and then remains nearly constant until the deck reaches a collapsing state. This behavior is due to the fact that CFRP sheets are elastic up to failure as observed in the laboratory tests.
3. The damping ratio of the concrete deck system does not change significantly with the severity of damage in the deck. Typically it ranges from 3% to 5%.
4. Skewness of bridge decks tends to increase the fundamental frequency of the decks. For a skewed deck of 15♭, the frequency increases about 7%. The fundamental frequency of the finite element model of the center span agrees with the test result. This ensures some confidence on the global feature of the computer model.

6. SWEPT-SINE DYNAMIC TESTS

6.1 INTRODUCTION

In the preceding sections, harmonic tests are used to determine the transfer function of a response quantity of RC structures. Both natural frequency and damping ratio of the structures can be identified from the transfer function. Frequency has been claimed in literature as an effective indicator to identify the severity of damage in structures. It was found in this study that the "resonant" frequency of the structures changes with the harmonic loading history if the structures are damaged severely. When a structure is subjected to a harmonic load and tested with the increasing or decreasing excitation frequencies (one frequency per test), the shift in the "resonant" frequency due to the different sequence of changing the excitation frequency is well corrected with the severity of damage. Therefore, the frequency shift is also a promising indicator for damage detection.

Each test using a sinusoidal load only contributes one point on the transfer function. Therefore harmonic tests are tedious and time consuming in laboratory or field conditions. To identify the natural frequency or the frequency shift could take more than one hour. Swept-sine tests are thus studied here to expedite the process. These tests can continuously sweep the structures' frequency in low-to-high and then high-to-low order. A smooth transfer function can then be drawn in a rather short period.

Swept-sine tests have been used to identify the natural frequency of various structures. However, to the best knowledge of the authors, using them to determine transfer functions originates from this study. In what follows, some theoretical developments are introduced. The transfer functions obtained from the swept-sine tests are then modified to determine the functions corresponding to harmonic tests. The natural frequency and the frequency shift are finally identified.

6.2 THEORETICAL ANALYSIS

6.2.1 Principle

Consider a simply supported beam subjected to a swept-sine dynamic load at midspan as shown in Figure 6.1. The load is generated by a shaker and can be determined

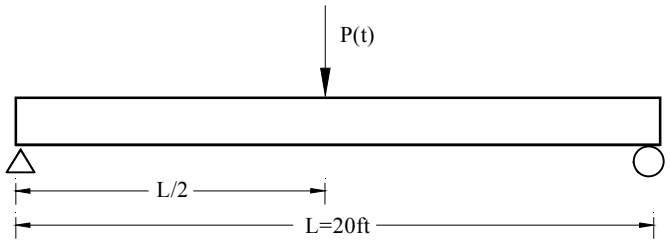

Figure 6.1 Example beam

by Eqs. (2.4) and (2.5). For swept-sine tests, however, the operating frequency Ω in Eq. (2.4) is a function of time *t*. For simplicity, the frequency is assumed to linearly increase and then decrease with time *t*. That is,

$$\Omega = 2\pi(b + r't) \tag{6.1}$$

where b is an initial frequency in Hz, and r' is the increasing or decreasing rate of the operating frequency. By substituting Eqs. (2.5) and (6.1) into Eq. (2.4), we have:

$$P(t) = 0.1322 \times (2\pi f)^2 \times \sin(\theta/2) \times \sin[2\pi(b + r't)t] \tag{6.2}$$

in which the operating speed of the shaker, corresponding to the excitation frequency in harmonic tests, can be expressed into:

$$f = \frac{d}{dt}(\Omega t) = b + 2r't \tag{6.3}$$

For convenience, let

$$r = 2r' \tag{6.4}$$

and r is the increasing or decreasing rate of the excitation frequency. Therefore the swept-sine dynamic load can be rewritten as:

$$P(t) = 0.1322 \times [2\pi(b + rt)]^2 \times \sin(\theta/2) \times \sin[2\pi(b + \frac{r}{2}t)t] \tag{6.5}$$

For a simply-supported beam, the natural frequency of the second mode is four times that of the fundamental mode. Furthermore, only one concentrated load is applied at midspan in this study, or at the node of the second mode. The first mode thus dominates the dynamic response of the beam. In what following, only the fundamental mode is included. The deflection and acceleration of the beam are computed using the Duhamel's integration method (Biggs, 1964).

A typical acceleration response at midspan is shown in Figure 6.2. If the excitation frequency f is increased or decreased slowly, the acceleration response in a short period is similar to the corresponding steady-state response of the beam under a harmonic load of frequency f. They are compared in Figure 6.3. Therefore, if r in Eq. (6.5) is properly selected, one swept-sine test can be used to replace a series of harmonic tests. A complete transfer function of the acceleration at midspan can be constructed in one swept-sine test. To determine the equivalent peak response due to a sinusoidal load, the relationship between two loads needs to be established. At a particular time instant, the excitation frequency and amplitude of a swept-sine load can respectively be determined by:

$$f = b + rt \tag{6.6}$$

and

$$A = 0.1322 \times [2\pi(b + rt)]^2 \times \sin(\theta/2) \tag{6.7}$$

The corresponding sinusoidal load at time t can be expressed into:

$$P_{\sin}(t) = A \times \sin(2\pi ft + c) \tag{6.8}$$

in which $c = -\pi rt^2$ is the phase difference between a swept-sine and a sinusoidal load at time t.

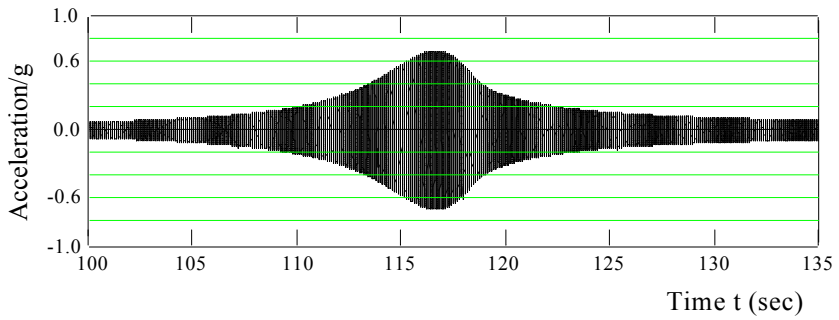

Figure 6.2 Analytical response at midspan of beam under swept-sine loading

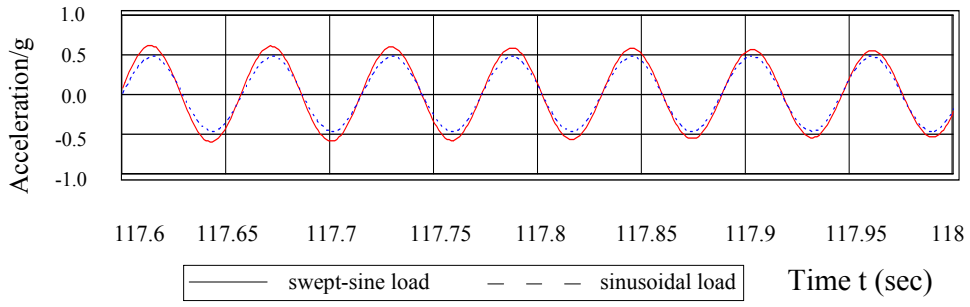

Figure 6.3 Response comparison under swept-sine and sinusoidal loads

6.2.2 Analysis Procedure

As indicated in Section 4, a transfer function of the response quantity of a RC structure under a harmonic load is used to identify the natural frequency and damping of the structure. Once the response of the structure subjected to a swept-sine load is obtained analytically or experimentally, the corresponding peak response under a sinusoidal load is therefore required. The procedure to determine this is rather simple as summarized below.

Step 1. Select a time instant t and a small window of the structural response under a swept-sine load in a symmetrical domain of time t. Typically three cycles before and after time t are used.

Step 2. Determine the time period of each cycle of vibration and the corresponding amplitude.

Step 3. Take an average of the time periods and amplitudes determined in Step 2, respectively, to obtain the period or frequency and the corresponding peak response at time t.

Step 4. Repeat Steps 1-3 until a complete transfer function is determined. This function is referred to as the unmodified transfer function.

The unmodified transfer function represents the resonant responses of a beam under a swept-sine load of varying amplitude. It has to be modified to obtain an equivalent function under harmonic loads of the constant amplitude (A_h) for the entire loading period. Therefore, the modification factor can be written as

$$MF = \frac{A_h}{A} \tag{6.9}$$

and the modified transfer function is equal to MF times the unmodified transfer function at each frequency (f). MF is evaluated at time t that is related to the frequency (f) by Eq. (6.7).

6.2.3 Relationship Between Responses Due To Swept-sine And Sinusoidal Loads

The aim of using swept-sine tests is mainly to minimize the time with reasonable accuracy to identify a transfer function. To understand how representative the swept-sine tests are to harmonic tests, the responses of a structure under a swept-sine load have to be related to those under harmonic loads. The shape and amplitude of a transfer function are primarily determined by the structural damping ratio (ζ) and natural frequency (ω_1) as well as the increasing or decreasing frequency rate (r). Both damping ratio and natural

frequency are the structure's properties and their effect on the structural responses is well understood (Biggs, 1964). In this report, emphasis is placed on the effect of the frequency rate (*r*).

A RC beam described in Section 3.1 is used as an example for analytical study. The modified acceleration transfer function under a swept-sine load of various frequency rates and that under harmonic loads are compared in Figure 6.4. It can be seen that the

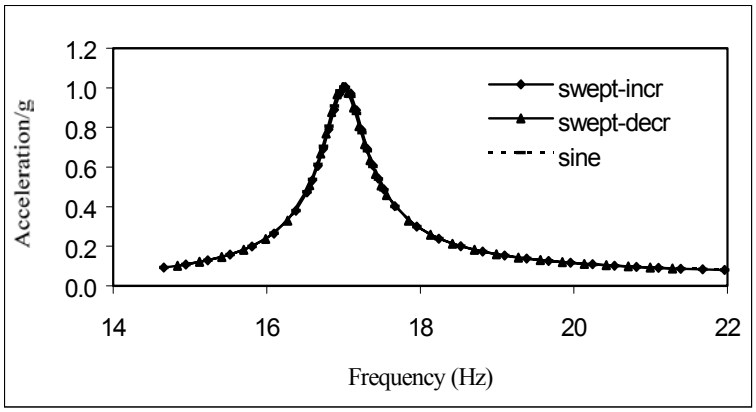

(a) r=0.014

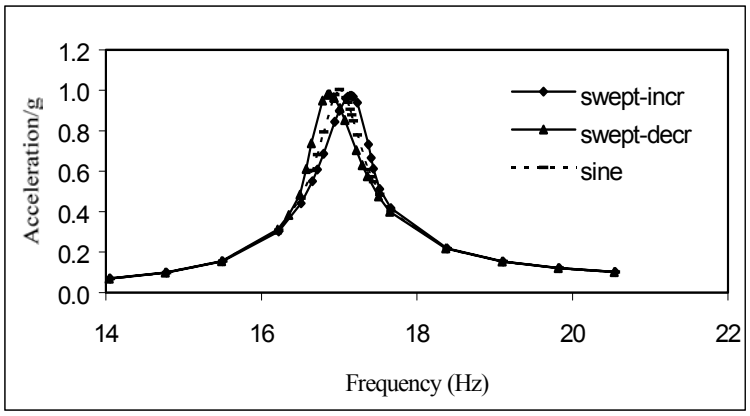

(b) r=0.144

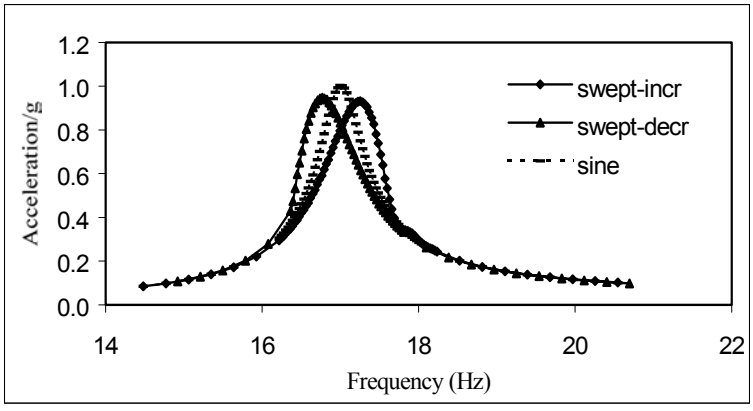

(c) r=0.289

Figure 6.4 Transfer functions from theoretical analysis

transfer functions of a beam under a swept-sine load of increasing or decreasing frequency are skewed to different sides of that under a harmonic load and their maximum responses decrease significantly as the frequency rate increases. However, both functions converge to the one under harmonic loads when the frequency rate is sufficiently low. Therefore, a single swept-sine test can be used to determine the complete transfer function as accurately as harmonic tests. The resonant frequency from the swept-sine tests shifts to the right of the natural frequency of the beam for the increasing excitation frequency and to the left for the decreasing excitation frequency part. As the frequency rate (r) increases, the error in resonant frequency becomes more pronounced. This mainly results from the delay in resonance. In harmonic tests, resonance occurs when an excitation frequency is tuned to the natural frequency of a beam as long as the beam vibrates for a sufficiently long time. However, the excitation frequency in swept-sine tests continuously changes with time so that resonance occurs at a later time after the excitation frequency sweeps through the natural frequency. It is also observed from Figure 6.4 that the resonant acceleration is slightly smaller for the increasing excitation frequency part than for the decreasing frequency part. This is because the applied force defined in Eq. (6.5) is proportional to the square of the excitation frequency. The dynamic response of a beam right before the resonance is then smaller for the increasing frequency part and therefore so is the maximum response in resonance.

To quantify the relationship between responses due to swept-sine and sinusoidal loads as shown in Figure 6.4, the resonant frequency, resonant acceleration and damping ratio are studied in more detail. The error in resonant frequency is normalized by the natural frequency of a beam and plotted in Fig 6.5 as a function of the excitation frequency rate (r). It is clearly observed that the amount of shift in resonant frequency, or relative error, is the same for both increasing and decreasing frequency parts. The relative error in resonant frequency varies nonlinearly with the frequency rate. The relative error can be mathematically written as

$$\delta f = \frac{\left| f_{swept} - f_{\sin e} \right|}{f_{\sin e}} \tag{6.10}$$

and it is related to r by

$$\delta f = 0.041 r^{0.845} \tag{6.11}$$

based on the best fit of numerical data. In Eq. (6.10), f_{swept} denotes the resonant frequency of a beam identified under a swept-sine load, and f_{sine} represents the resonant frequency under harmonic loads or natural frequency of the beam. When f_{swept} is identified from swept-sine tests, f_{sine} can then be determined from Eqs. (6.10) and (6.11).

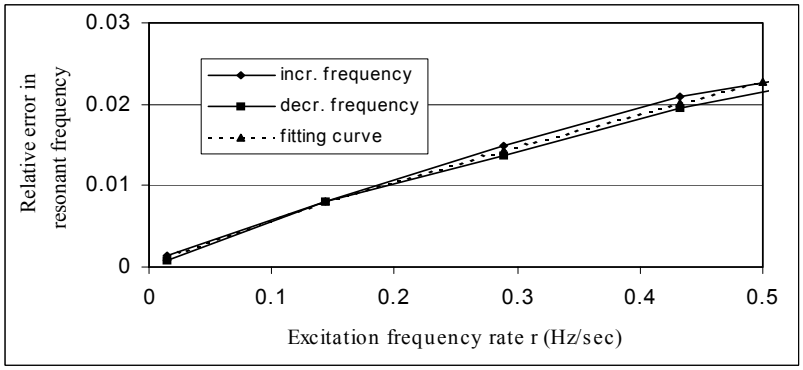

Figure 6.5 Effect of excitation frequency rate on resonant frequency

Similarly, the relative errors in resonant acceleration (δA) and damping ratio ($\delta\zeta$) are respectively calculated by

$$\delta A = \frac{\left|A_{swept} - A_{\sin e}\right|}{A_{\sin e}} \tag{6.12}$$

$$\delta\zeta = \frac{\left|\zeta_{swept} - \zeta_{\sin e}\right|}{\zeta_{\sin e}} \tag{6.13}$$

in which A_{swept} and A_{sine} represent the resonant responses of a beam under a swept-sine and a sinusoidal load. ζ_{swept} and ζ_{sine} are the damping ratios of the beam identified from the respective transfer functions. Figure 6.6 shows the relative error in resonant acceleration as a function of the frequency rate (r). It can be seen that the error increases nonlinearly as the frequency rate increases for both increasing and decreasing excitation frequency parts, and so does the deviation between two parts. The relation between the error and the frequency rate can be determined by curve fitting as

$$\delta A_{incr} = 0.23 r^{1.155} \qquad \text{for increasing frequency part} \tag{6.14}$$

$$\delta A_{decr} = 0.3 r^{1.155} \qquad \text{for decreasing frequency part} \tag{6.15}$$

where δA_{incr} and δA_{decr} are the resonant acceleration errors corresponding to the increasing and decreasing frequency parts, respectively. When A_{swept} is identified from swept-sine tests, A_{sine} can then be determined from Eqs. (6.14) and (6.15).

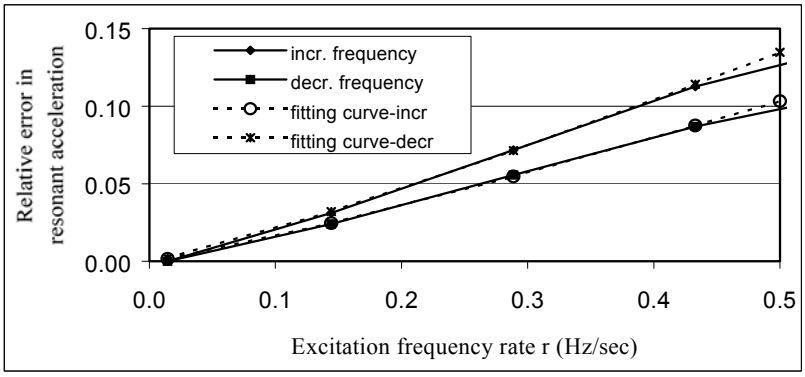

Figure 6.6 Effect of excitation frequency rate on resonant acceleration at midspan

The relation between the relative error in damping ratio ($\delta\zeta$) and the frequency rate (r) is presented in Figure 6.7. As r increases, the error in damping ratio increases for both increasing and decreasing frequency parts. Their relation can be expressed by the following equation:

$$\delta\zeta_{incr} = 1.261 r^{1.320} \qquad \text{for increasing frequency part} \tag{6.16}$$

$$\delta\zeta_{decr} = 1.230 r^{1.131} \qquad \text{for decreasing frequency part} \tag{6.17}$$

where $\delta\zeta_{incr}$ and $\delta\zeta_{decr}$ respectively denote the relative errors in damping ratio for two parts. When ζ_{swept} is identified from swept-sine tests, ζ_{sine} can then be determined from Eqs. (6.16) and (6.17).

As discussed above and illustrated in Figures. 6.5 to 6.7, the error in resonant frequency, damping ratio and resonant response all become considerably larger as the frequency rate r increases. In order to obtain results more representative to those under

harmonic loads, the frequency rate shall be limited. In addition, beating may occur when r is in a certain range as shown in Figure 6.8. Such a phenomenon will not be present under harmonic loads and thus makes it impossible to establish a relation between swept-sine and sinusoidal tests. Based on extensive analytical results, a swept-sine test with r less than 0.5 seems to be a good representation to a series of harmonic tests. This threshold approximately corresponds to a dimensionless ratio ($1000r/f_1^2$) of 1, in which f_1 is the fundamental frequency of the RC beam.

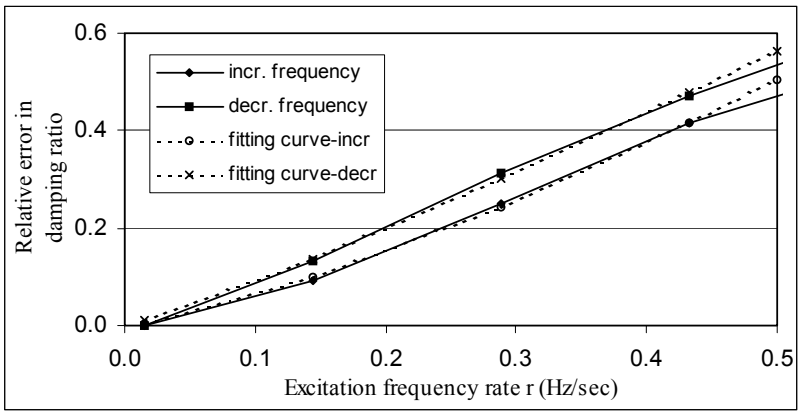

Figure 6.7 Effect of excitation frequency rate on damping ratio

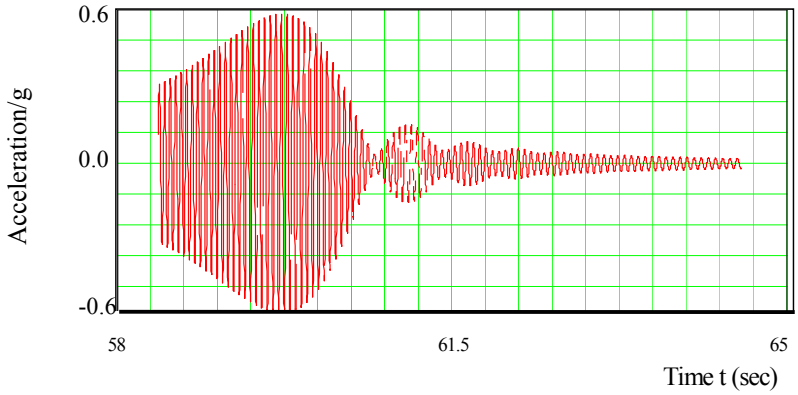

Figure 6.8 Beat phenomenon (r=1.443)

6.3 EXPERIMENTAL ANALYSIS

Swept-sine dynamic tests were conducted on Beams 2 and 3. The dynamic load is generated by the same shaker as used in harmonic tests. The excitation frequency ranges from 0 to 30 Hz for all swept-sine tests. By adjusting the time to accelerate and/or decelerate the speed of the electric motor, various frequency rates (r) can be set for different cases. An instrumentation scheme similar to harmonic tests was developed and the peak accelerations from the tests are compared with the analytical results presented in the preceding section.

6.3.1 Test Procedure and Plan

The same procedure as summarized in Section 3.4 was used during the swept-sine tests except that the dynamic force described in Eq. (6.5) is generated and the transient

responses are recorded. The frequency rate was adjusted with a control panel by setting different acceleration and deceleration time in the frequency range (0, 30 Hz). Swept-sine tests were carried out for two specimens: Beam 2 and Beam 3. Several tests were run on Beam 2 at the virgin state. For Beam 3, six runs were done after the beam was first subjected to 26 kips. For all test cases, swept-sine tests were always performed after several cycles of sinusoidal tests had been finished. Each test case is described in detail in Table 6.1.

Table 6.1 Case Descriptions of Swept-sine Tests

Case	Loading Stage	Number of Tests
1	No static load was ever applied on Beam 2. The beam is in its virgin state and behaves elastically	5 tests were conducted. Each corresponds to a rising time of 30 sec, 60 sec. 100 sec, 150 sec or 200 sec from 0 to 30 Hz and a short decaying time.
2	A static load (26 kips) was applied on Beam 3 but it was removed during the dynamic test. The reinforcement in the beam is yielding.	6 tests were carried out. Each corresponds to the same rising and decaying time of 10 sec, 20 sec, 40 sec, 80 sec, 160 sec or 200 sec.

6.3.2 Test Results and Analysis

Figure 6.9 shows the acceleration response at midspan of the beam for various cases and frequency rates. It is obvious that the beat phenomenon has occurred in Case 2 when r is equal to 2.792 and 2.587, respectively, for the increasing and decreasing frequency parts. Under other conditions, the acceleration envelope varies with time much more smoothly. A closeup of a small period of the response from the tests is plotted in Figure 6.10. As one can see, this period of response closely follows the steady-state response under a harmonic load. Around an instant t, one can read the time elapsed in each cycle of vibration. The average of the time for six consecutive cycles is considered as the excitation period at time t, from which the excitation frequency can be calculated. After a dozen of readings at various instances, the excitation frequency can be related to time t as illustrated in Figure 6.11 for Cases 1 and 2. Obviously, it varies linearly with time t as described in Eq. (6.6). Due to the high frequency decaying rate for Case 1 and lack of the steady-state response for increasing frequency in Case 2, that part of the response is not reliable and will not be discussed further. The average peak responses of six cycles of vibration centered at time t can also be found in the same function. Such a plot between the average peak response and the excitation frequency shows the unmodified transfer function as discussed in Section 6.2.2. The modified transfer function determined by multiplying the unmodified with the factor described in Eq. (6.9) is presented for each case in Figures 6.12 and 6.13, together with the corresponding results from harmonic tests. In general, the transfer function from a swept-sine test ($r \leq 0.5$) and a series of harmonic tests are almost identical, indicating that a single swept-sine test can be used to construct a complete transfer function for Case 1. For Case 2, however, the swept-sine tests did not capture the transient characteristics associated with the nonlinear vibration of cracked RC beams as pointed out in Section 4.2.4. This is primarily because all swept-sine tests were conducted after a series of harmonic tests. As a result, the transient surface condition along cracks becomes stationary and the beam actually vibrates in a linear fashion. A complete set of transfer functions from the swept-sine tests are attached in Appendix E and F.

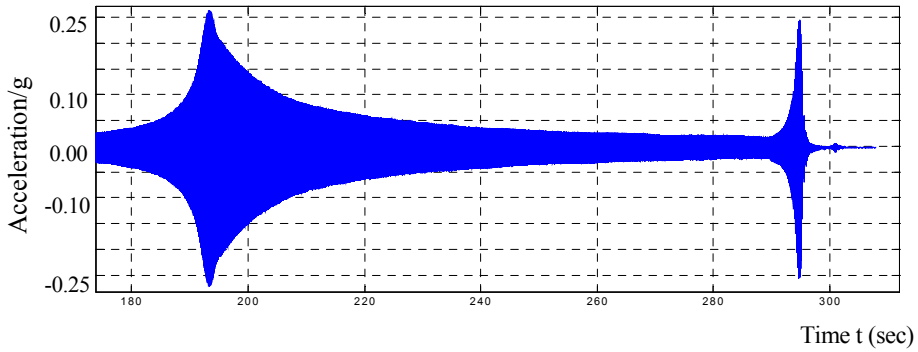

(a) Case 1: Increasing frequency rate, r=0.117; decreasing frequency rate, r=1.789

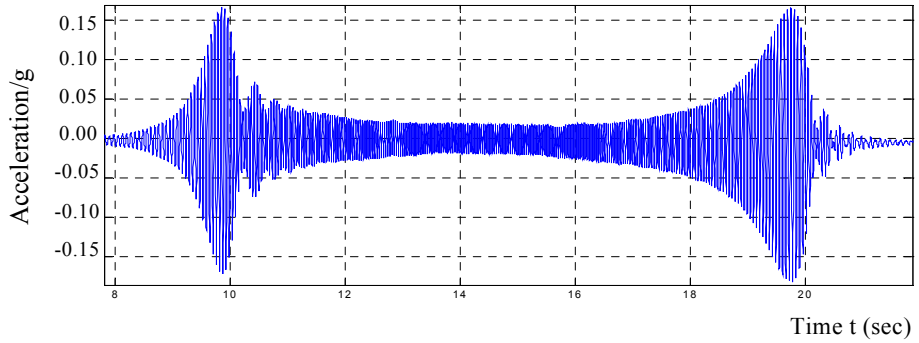

(b) Case 2: Increasing frequency rate, r=2.792; decreasing frequency rate, r=2.587

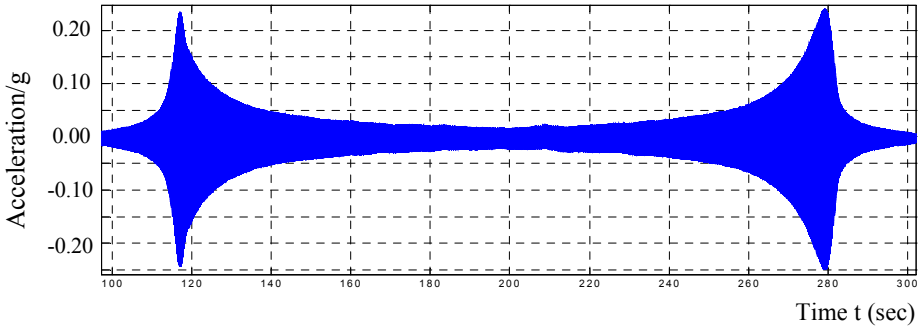

(c) Case 2: Increasing frequency rate, r=0.144; decreasing frequency rate, r=0.149

Figure 6.9 Acceleration at midspan from swept-sine tests

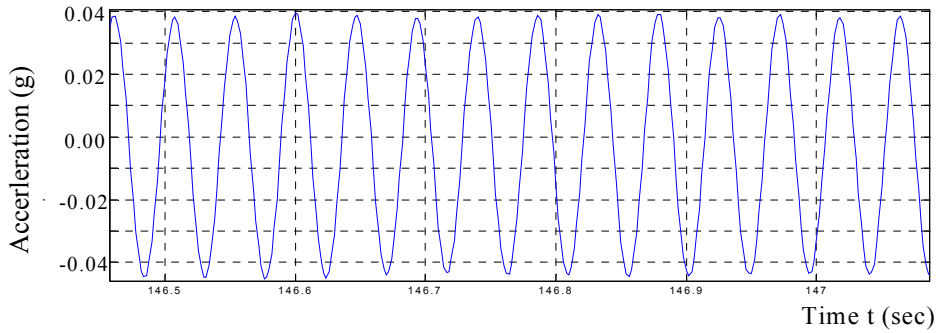

Figure 6.10 Closeup on acceleration response

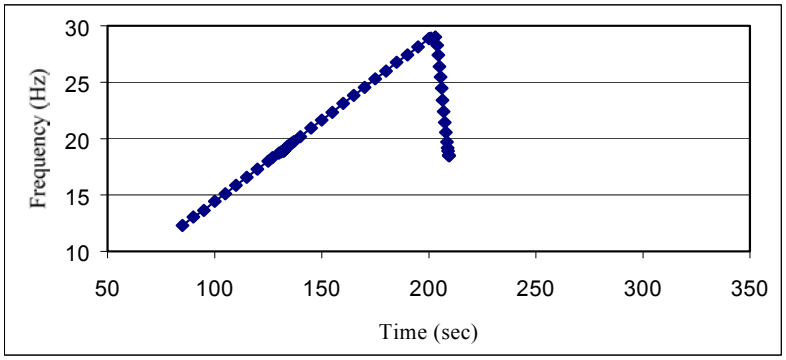

(a) Case 1

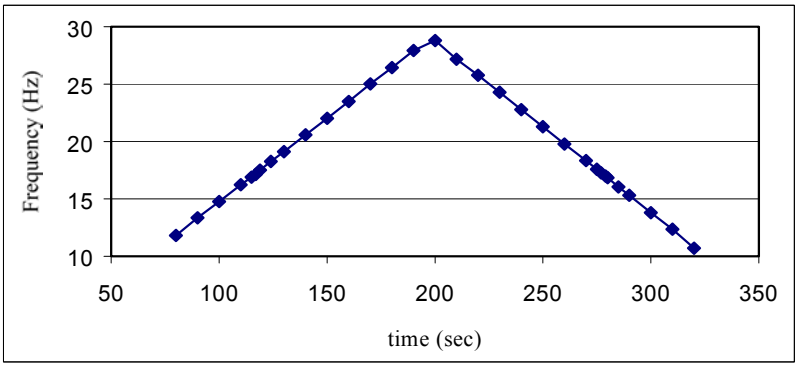

(b) Case 2

Figure 6.11 Excitation frequency vs. time

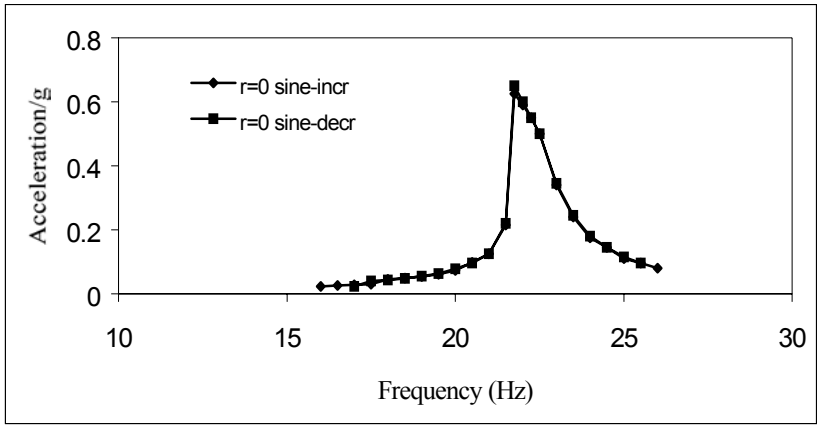

(a)

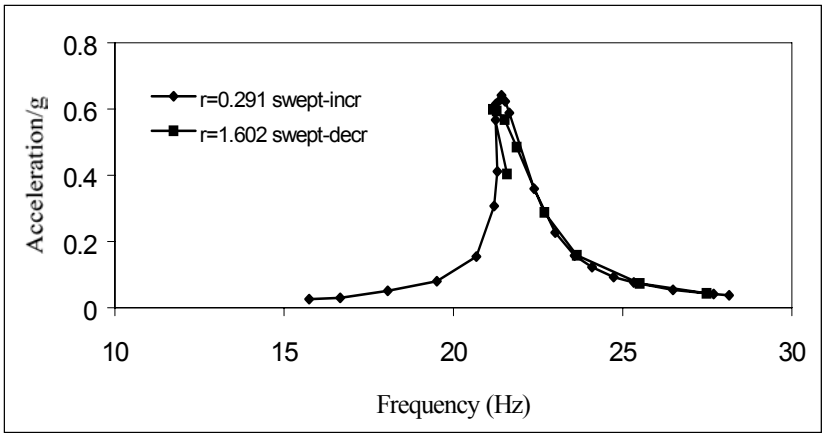

(b)

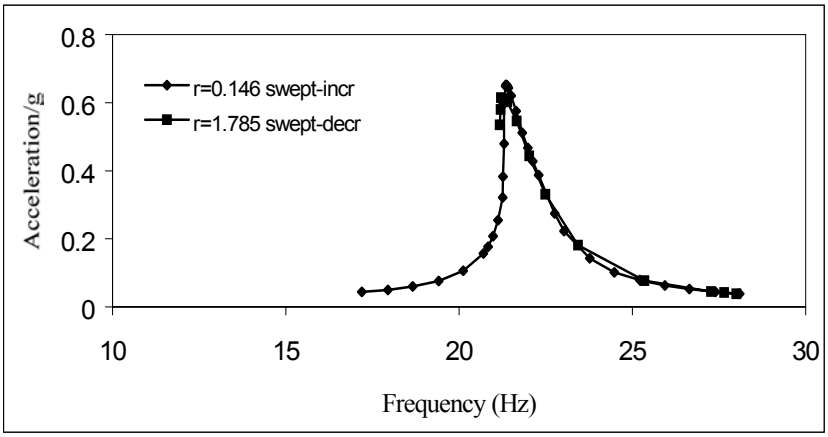

(c)

Figure 6.12 Transfer functions for Case 1 from test results

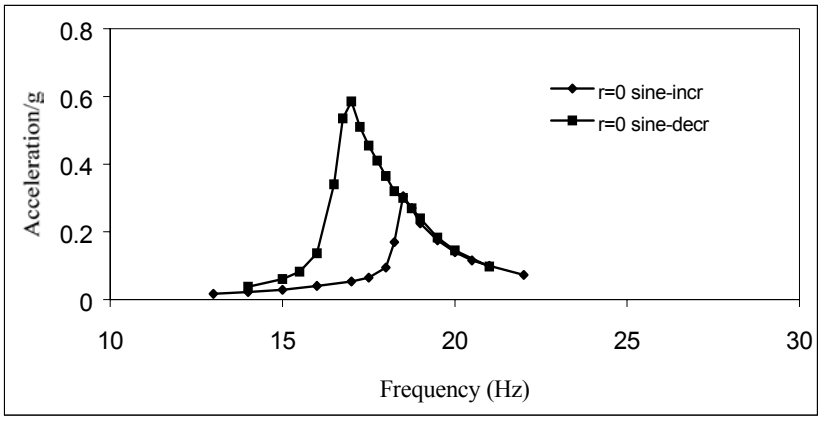

(a)

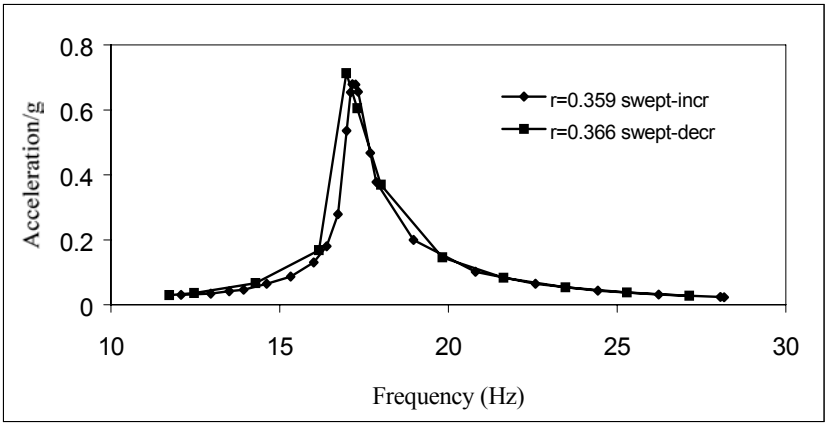

(b)

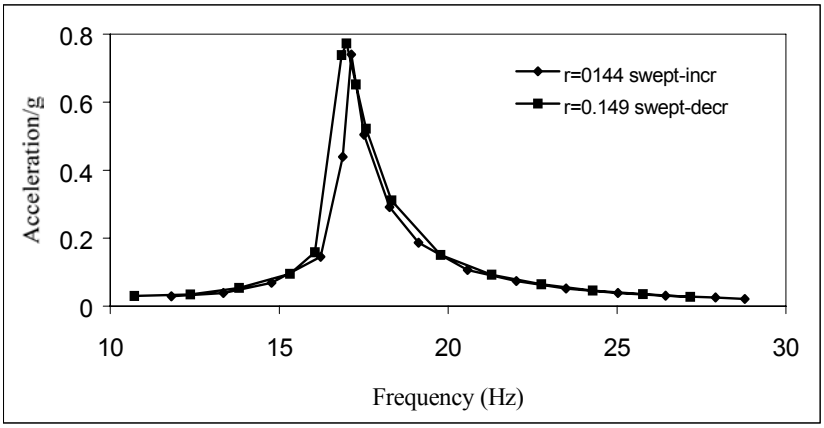

(c)

Figure 6.13 Transfer functions for Case 2 from test results

For two cases described in Table 6.1, the resonant frequency, resonant acceleration and damping ratio are summarized in Tables 6.2 and 6.3 for the increasing excitation frequency part in Case 1 and the decreasing excitation frequency part in Case 2. Those predicted by Eqs. (6.11) and (6.14) to (6.17) as well as the harmonic test results

are also included in the tables. The predicted results are supposed to be equivalent to those from the harmonic tests. It is observed from Tables 6.2 and 6.3 that the predicted resonant frequencies are indeed in a good agreement with the experimental results from harmonic tests. However, the predicted acceleration is larger in Case 1 and significantly larger in Case 2 than the corresponding experimental result from harmonic tests. On the contrary, the predicted damping is smaller than the test results. The main reason for the appreciable deviation is because the maximum response is often missed during the harmonic tests. This is especially so for the cracked RC beam (Case 2) due to the unstable condition along the crack surface. The resonant accelerations for the increasing frequency part in Case 1 and the decreasing part in Case 2 are modified based on the understanding of a typical transfer function of a linear system as shown in Figure 2.2. The modified acceleration and the corresponding damping ratio are also listed in Tables 6.2 and 6.3. It can be seen that the predicted results by Eqs. (6.11) and (6.14) to (6.17) agree fairly well with the modified test results. This indicates that the equations of (6.11) and (6.14) to (6.17) are sufficiently accurate in predicting the frequency and damping of RC structures and their responses from a single swept-sine test.

Table 6.2 Swept-sine vs. Harmonic Tests: Case 1 Increasing Excitation Frequency

	Frequency rate r (Hz/sec)	Resonant frequency (Hz)	Resonant acceleration (g)	Damping ratio
Harmonic test	0	21.75/21.76[a]	0.625/0.66[a]	0.023/0.016[a]
Swept-sine test	0.146	21.38/21.20[b]	0.646/0.66[c]	0.017/0.015[d]
	0.193	21.35/21.13[b]	0.649/0.67[c]	0.017/0.015[d]
	0.291	21.43/21.13[b]	0.632/0.67[c]	0.017/0.014[d]

Note: a. Modified results from harmonic tests
b. Predicted results by Eq. (6.11) from swept-sine tests
c. Predicted results by Eq. (6.14) from swept-sine tests
d. Predicted results by Eq. (6.16) from swept-sine tests

Table 6.3 Swept-sine vs. Harmonic Tests: Case 2 Decreasing Excitation Frequency

	Frequency rate r (Hz/sec)	Resonant frequency (Hz)	Resonant acceleration (g)	Damping ratio
Harmonic test	0	17/16.9[a]	0.585/0.66[a]	0.033/0.023[a]
Swept-sine test	0.149	16.98/17.12[b]	0.772/0.80[c]	0.024/0.021[d]
	0.183	16.94/17.11[b]	0.749/0.78[c]	0.024/0.021[d]
	0.366	16.94/17.24[b]	0.713/0.79[c]	0.026/0.020[d]

Note: a. Modified results from harmonic tests
b. Predicted results by Eq. (6.11) from swept-sine tests
c. Predicted results by Eq. (6.15) from swept-sine tests
d. Predicted results by Eq. (6.17) from swept-sine tests

To compare the experimental with the predicted results by Eqs. (6.11) and (6.14 to 6.17), Figs. 6.14 to 6.16 reproduce the relative error in resonant acceleration, resonant frequency and damping ratio from theoretical analysis as shown in Figs. 6.5 to 6.7 together with the swept-sine (modified) and harmonic test results for Cases 1 and 2. In

general, the analytical results reasonably well agree with the experimental results as long as the frequency rate (r) is less than 0.25. As r increases, the theoretical prediction significantly deviates from the test results, in particular for the resonant frequency identified from the swept-sine tests with decreasing excitation frequency. In light of the theoretical analysis discussed in Section 6.2.3 and the experimental verification above, we recommend that $2000r/f_1^2$ be less than 1.0 for practical applications.

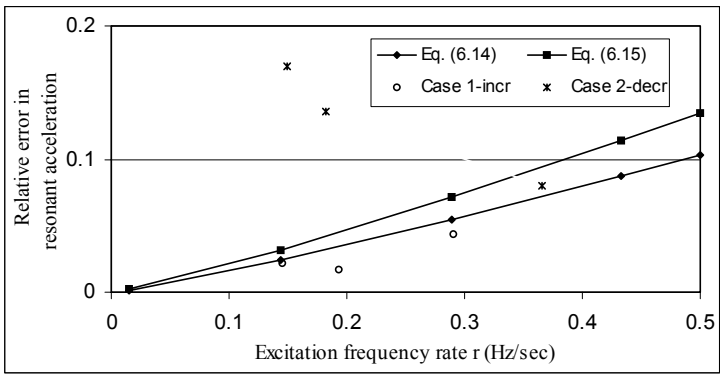

Figure 6.14 Relative error in resonant acceleration from analysis and swept-sine tests

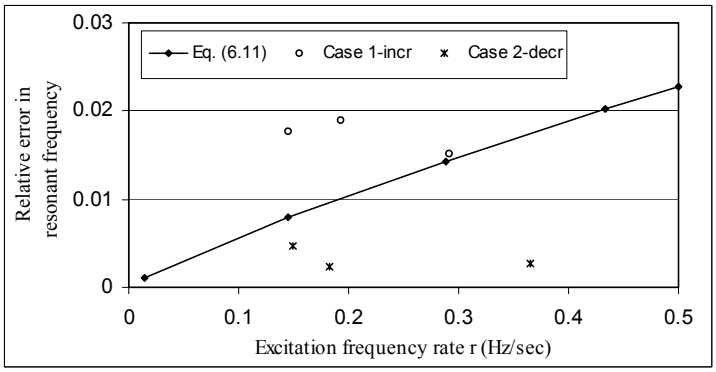

Figure 6.15 Relative error in resonant frequency from analysis and swept-sine tests

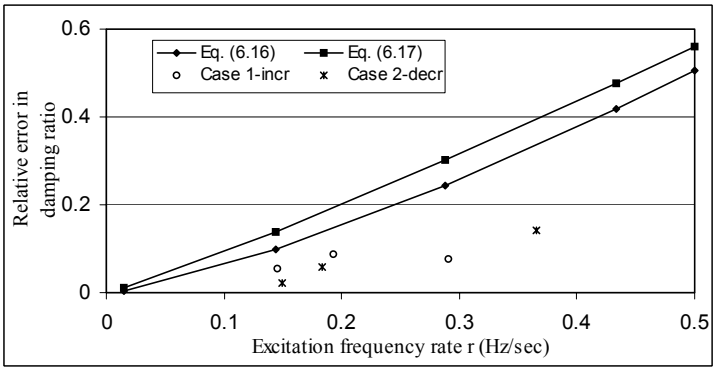

Figure 6.16 Relative error in damping ratio from analysis and swept-sine tests

6.4 CONCLUSIONS

Based on the extensive analysis and experimental verification, the following conclusions can be drawn:

1 When the frequency rate of swept-sine loads is sufficiently small, a single swept-sine test can be used to determine the natural frequency, damping ratio and resonant responses of a beam. Beating phenomenon appears immediately after resonance when a beam is subjected to a swept-sine load with rapidly increasing and decreasing excitation frequencies.

2 The resonant responses, resonant frequencies and damping ratios of a beam under harmonic loading can be respectively predicted from Eqs. (6.11) and (6.14) to (6.17) based on the experimental results from a swept-sine test. These relations have been proved to be reasonably accurate for a low excitation frequency rate.

3 For practical applications, the frequency rate of swept-sine loading should be limited to $f_1^2/2000$ in which f_1 represents the fundamental frequency of the structure under study.

7. SUMMARY AND RECOMMENDATIONS

Dynamic signature tests have been conducted on three RC beams in lab and a solid bridge deck in field condition. One beam is strengthened with externally-bonded CFRP sheets. Both sinusoidal and swept-sine loads are used for the dynamic tests of beams. Based on this study, the following conclusions can be drawn:

1. The fundamental frequency and modal damping ratio of RC beams, uncracked or cracked, can be identified with reasonable accuracy. The fundamental frequency of a damaged RC beam can be well correlated with the severity of damage and can therefore serve as an effective indicator for damage detection.
2. Dynamic signatures (natural frequency and damping) of a newly damaged RC beam are time dependent but can be easily identified by applying a preload on the beam during the tests. The net effect of the preload is to keep micro-cracks in the beam open during the vibration tests.
3. Two transfer functions of a newly damaged beam significantly differ from each other in magnitude and shape when the beam is tested under a harmonic load with the excitation frequency increasing vs. decreasing in sequence. Their corresponding resonant frequencies and damping ratios are also quite different. The shift in resonant frequency significantly increases with the severity of damage and responds to the unstable surface condition along micro cracks. This frequency shift is thus a promising indicator for detecting and locating the damage in RC structures when the structure condition is unknown before the test. The damping ratio of the beam is larger when tested with the decreasing excitation frequency. The similar trend in frequency shift has been observed in the bridge test but the magnitude of the shift is significantly smaller due to the complexity of a skewed deck system.
4. The derived theoretical formula accounting for the preload effect is in excellent agreement with the test data regardless of the state of damage occurring in RC structures. The theoretical prediction on the fundamental frequency using the equivalent moment of inertia also agrees very well with the experimental results.
5. The fundamental frequency of a CFRP strengthened beam considerably decreases at the initiation of cracking in concrete material and then remains nearly constant until the beam completely collapses. This behavior is due to the fact that CFRP sheets are elastic up to failure. This observation has been verified the bridge test even though it is less obvious. On the other hand, the fundamental frequency of RC beams without CFRP strengthening decreases continuously as the beams experience concrete cracking, reinforcement yielding and a complete failure.
6. The damping ratio of the tested RC beams ranges from 3% to 4% while that of the bridge deck system is about 3-5%.
7. The fundamental frequency of the bridge deck from the computer model matches with that from the bridge test. The skew effect of Bridge J857 on the fundamental frequency is about 7% based on the computer simulation.
8. A single swept-sine test can be conducted to replace a series of harmonic tests. Therefore, tremendous time and effort can be saved by using swept-sine tests to determine the transfer function of RC structures in laboratory and field applications.

9. The relations between the transfer functions from harmonic and swept-sine tests are established analytically and validated through test data. They can be used with reasonable accuracy to determine the resonant response, resonant frequency and damping ratio of a structure from the experimental results of a swept-sine test.
10. To ensure the accuracy in the identification of eigenproperties of structures, it is recommended that the frequency rate used in swept-sine tests be less than $f_1^2/2000$ for practical applications.

As a feasibility study on the dynamic signature tests, this project fulfills its original goal. However, further investigations are required to verify how to effectively use the fundamental frequency for the damage detection of other RC structures and to fully develop the new damage indicator, frequency shift, for newly-damaged structures. It is also critical to develop a theoretical model for analyzing a moderately-damaged RC beam that is subjected to strong nonlinear vibration under harmonic loads. For practical applications, it is pertinent to use a swept-sine test to determine the shift in resonant frequency. Future research will be pursued in these areas.

8. REFERENCES

Adams, R. D., et al (1975), Vibration Testing as a Nondestructive Test Tool for Composite Materials, Composite Reliability, ASTM STP 580, pp159-175.

Aktan, A. E. and Lee, K. L. (1994), Modal testing for structural identification and condition assessment of constructed facilities. Proc. of 12th international modal analysis conference pp462-468.

American Concrete Institute (1999), Building code requirements for reinforced concrete (ACI 318-99), American Concrete Institute, Detroit, Michigan, June.

Bazant, Z. P.and Byung, H OH. (1984), Deformation of progressively cracking reinforced concrete beams, ACI Structural Journal, May-June, pp268-278.

Biggs, J. M. (1964), Introduction to structural dynamics, McGraw-Hill.

Chang, F. G., ed. (1997), Structural health monitoring: current status and perspectives, Technomic Publishing, Inc.

Doebling, S. W., et al (1996), Damage identification and health monitoring of structural and mechanical systems from changes in their vibration characteristics: a literature review, LA-13070-MS, Los Alamos National Laboratory, New Mexico.

Ewins, D. J. (1984), Model testing: Theory and Practice, Research Studies Press.

James, M. L., et al (1994), Vibration of Mechanics and Structural Systems, 2nd Ed, Harper Collins College Publishers.

Lyon, R. (1995), Structural diagnostics using vibration transfer functions, Sound and Vibration, 29(1), pp28-31.

Mayo, R. (1999), Strengthening of bridge G-270 with externally bonded CFRP sheets, MS thesis, Department of Civil Engineering, University of Missouri-Rolla.

Mazurek, D. F.and Dewolf, J. T. (1990), Experimental study of bridge monitoring technique, ASCE , Journal of Structural Engineering, Vol. 116, No. 9, pp2532-2549.

Mbrace™ (1998), Composite Strengthening System, Engineering Design Guidelines, Second Edition. Structural Preservation Systems, Inc.

Salastan, J. and Pietrzko, S. (1993), Changes of RC beam modal parameters due to cracks, Proc. of the 11th international modal analysis conference, pp70-76.

Salawu, O. S. (1997), Detection of structural damage through changes in frequency; a review. Engineering Structures, 19(9), pp718-723.

Salawu, O. S. (1994), Nondestructive evaluation of constructed facilities using vibration testing, Insight, 36(8), pp611-615.

Salawu, O. S. and Williams, C. (1995), Bridge assessment using forced-vibration testing, Journal of Structural Engineering, ASCE, 121(2), pp161-173.

Samman, S. S. and Biswas, M. (1994), Vibration testing for nondestructive evaluation of bridges, Journal of Structural Engineering, ASCE, 120(1), pp290-306.

Sanayei, M. and Onipede, O. (1991), Damage assessment of structures using static test data. AIAA, 29(7), pp1174-1179.

Sanders, D., Kim, Y. I., and Stubbs, R. N. (1992), Nondestructive evaluation of damage in composite structures using modal parameters, Experimental Mechanics, 32, pp240-251.

Schulz, M. J., Pai, P. F., and Abdelnaser, A. S. (1996), Frequency response function assignment technique for structural damage identification, Proc. of the 14th international modal analysis conference, pp1285-1291.

Stubbs, N. and Osegueda, R. (1993), Global nondestructive damage evaluation of offshore platforms using modal data, Proc. of the 6th international offshore mechanics arctic engineering, pp517-524.

Wang, Z, Man, X. C., Finch, R. D., and Jansen, B. H. (1998), The dyanmic behavior and vibration monitoring of RC beams, ASTM Journal of Testing and Evaluation, JTEVA, Vol 26, No. 5, pp405-419.

Yao, G. C., Chang K. C., and Lee G. C. (1992), Damage diagnosis of steel frames using vibration signature analysis. ASCE Journal of Structural Engineering, Vol 118, No. 9, pp1949-1961.

APPENDIX A:

TRANSFER FUNCTIONS OF BEAM 1

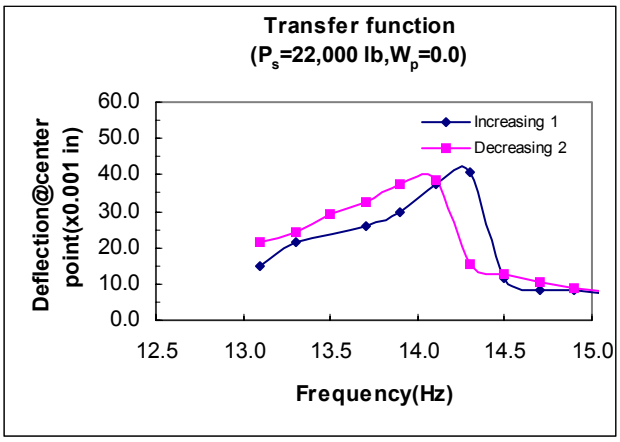
Transfer function
(Ps=22,000 lb,Wp=0.0)
Deflection@center point(x0.001 in)
60.0
50.0
40.0
30.0
20.0
10.0
0.0
12.5
13.0
13.5
14.0
14.5
15.0
Frequency(Hz)
Increasing 1
Decreasing 2

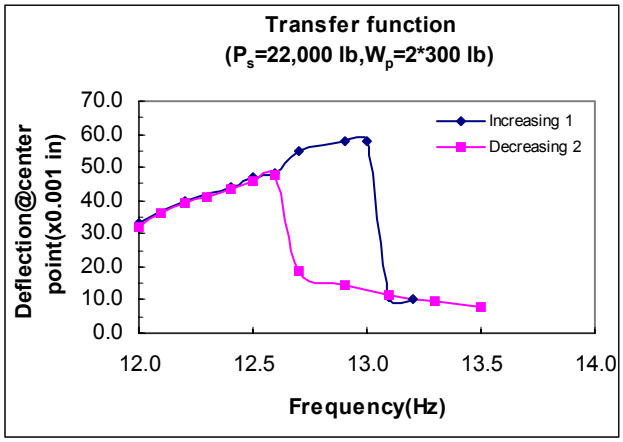
Transfer function
(Ps=22,000 lb,Wp=2*300 lb)
Deflection@center point(x0.001 in)
70.0
60.0
50.0
40.0
30.0
20.0
10.0
0.0
12.0
12.5
13.0
13.5
14.0
Frequency(Hz)
Increasing 1
Decreasing 2

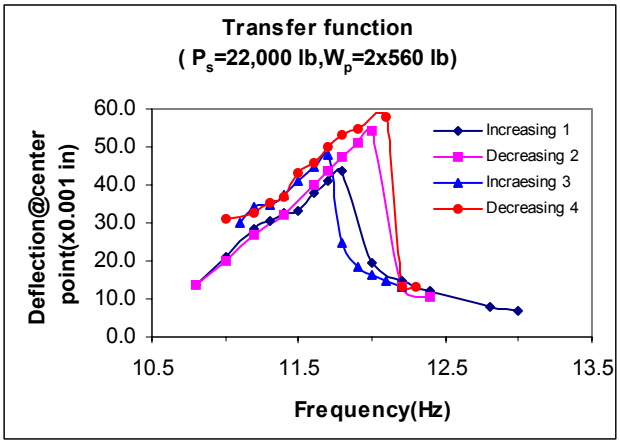
Transfer function
(Ps=22,000 lb,Wp=2x560 lb)
Deflection@center point(x0.001 in)
60.0
50.0
40.0
30.0
20.0
10.0
0.0
10.5
11.5
12.5
13.5
Frequency(Hz)
Increasing 1
Decreasing 2
Incraesing 3
Decreasing 4

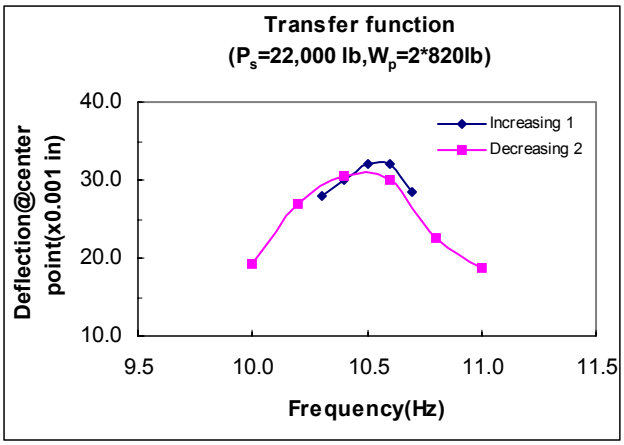
Transfer function
(Ps=22,000 lb,Wp=2*820lb)
Deflection@center point(x0.001 in)
40.0
30.0
20.0
10.0
9.5
10.0
10.5
11.0
11.5
Frequency(Hz)
Increasing 1
Decreasing 2

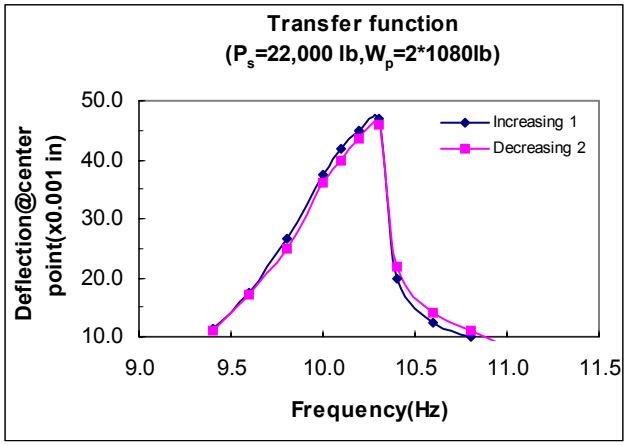
Transfer function
(Ps=22,000 lb,Wp=2*1080lb)
Deflection@center point(x0.001 in)
50.0
40.0
30.0
20.0
10.0
9.0
9.5
10.0
10.5
11.0
11.5
Frequency(Hz)
Increasing 1
Decreasing 2

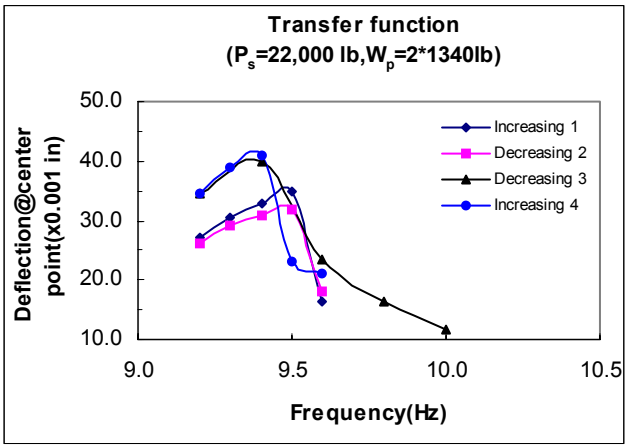
Transfer function
(Ps=22,000 lb,Wp=2*1340lb)
Deflection@center point(x0.001 in)
50.0
40.0
30.0
20.0
10.0
9.0
9.5
10.0
10.5
Frequency(Hz)
Increasing 1
Decreasing 2
Decreasing 3
Increasing 4

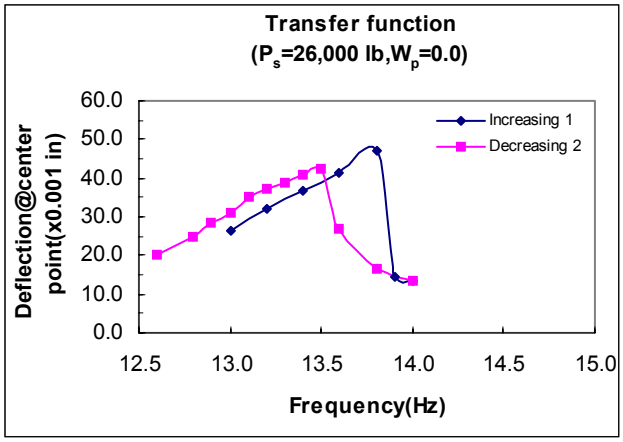
Transfer function
(Ps=26,000 lb,Wp=0.0)
Deflection@center point(x0.001 in)
60.0
50.0
40.0
30.0
20.0
10.0
0.0
12.5
13.0
13.5
14.0
14.5
15.0
Frequency(Hz)
Increasing 1
Decreasing 2

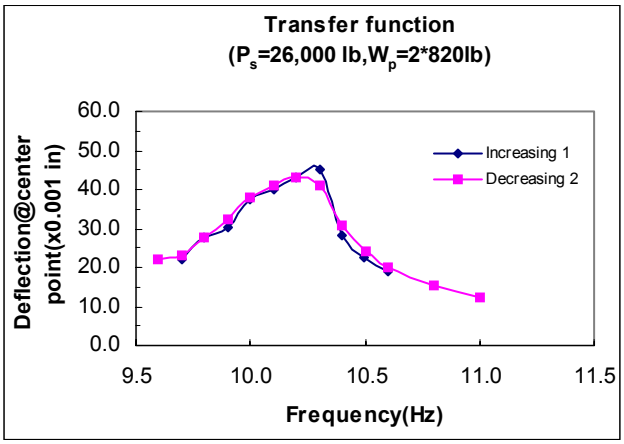
Transfer function
(Ps=26,000 lb,Wp=2*820lb)
Deflection@center point(x0.001 in)
60.0
50.0
40.0
30.0
20.0
10.0
0.0
9.5
10.0
10.5
11.0
11.5
Frequency(Hz)
Increasing 1
Decreasing 2

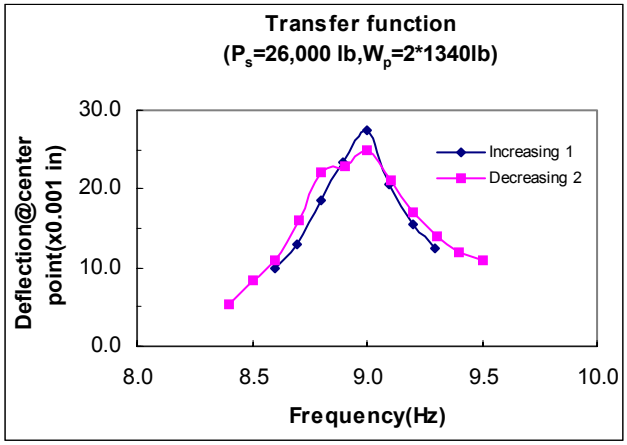
Transfer function
(Ps=26,000 lb,Wp=2*1340lb)
Deflection@center point(x0.001 in)
30.0
20.0
10.0
0.0
8.0
8.5
9.0
9.5
10.0
Frequency(Hz)
Increasing 1
Decreasing 2

APPENDIX B:

TRANSFER FUNCTIONS OF BEAM 2

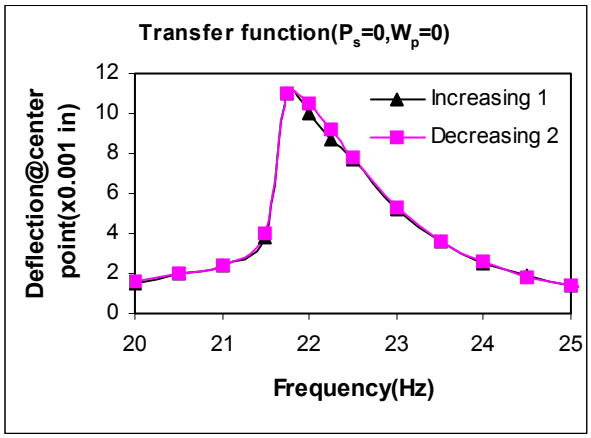
Transfer function(P_s=0,W_p=0)
Deflection@center point(x0.001 in)
Increasing 1
Decreasing 2
Frequency(Hz)
0
2
4
6
8
10
12
20
21
22
23
24
25

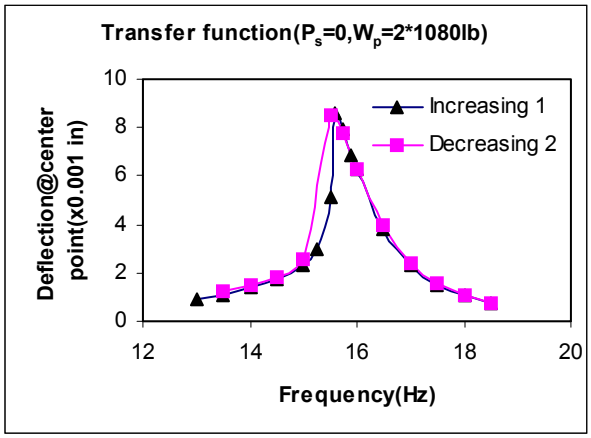
Transfer function(P_s=0,W_p=2*1080lb)
Deflection@center point(x0.001 in)
Increasing 1
Decreasing 2
Frequency(Hz)
0
2
4
6
8
10
12
14
16
18
20

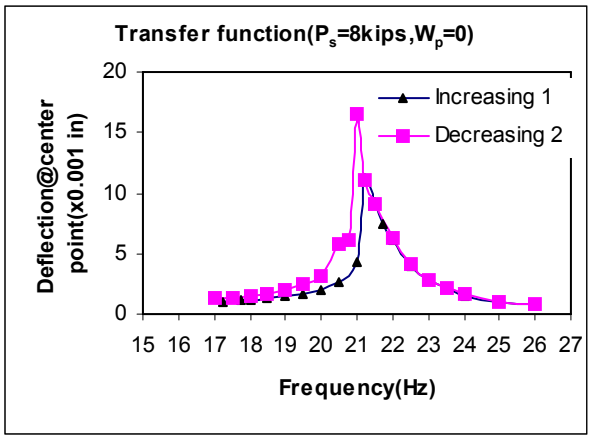
Transfer function(P_s=8kips,W_p=0)
Deflection@center point(x0.001 in)
Increasing 1
Decreasing 2
Frequency(Hz)
0
5
10
15
20
15 16 17 18 19 20 21 22 23 24 25 26 27

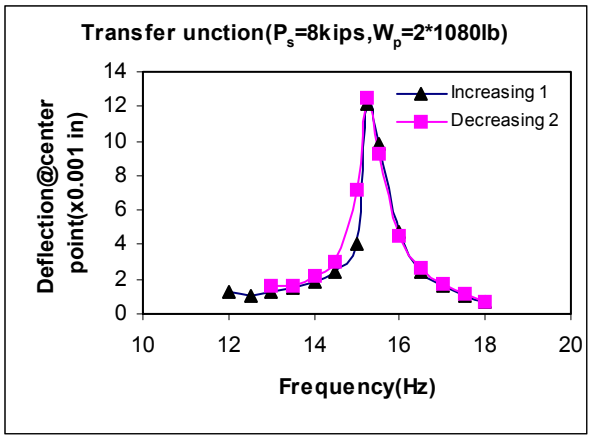
Transfer unction(Ps=8kips,Wp=2*1080lb)
Deflection@center point(x0.001 in)
Frequency(Hz)
Increasing 1
Decreasing 2
0
2
4
6
8
10
12
14
10
12
14
16
18
20

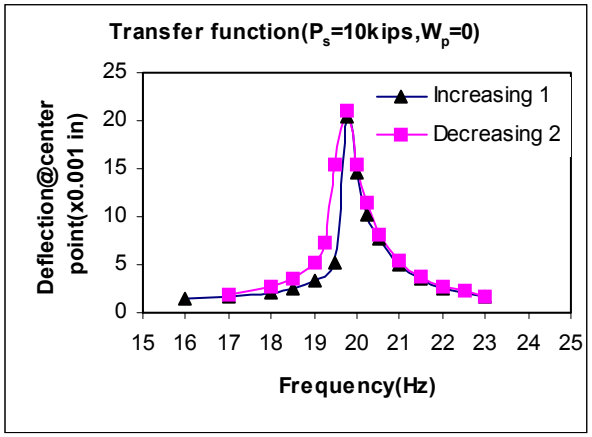
Transfer function(Ps=10kips,Wp=0)
Deflection@center point(x0.001 in)
Frequency(Hz)
Increasing 1
Decreasing 2
0
5
10
15
20
25
15
16
17
18
19
20
21
22
23
24
25

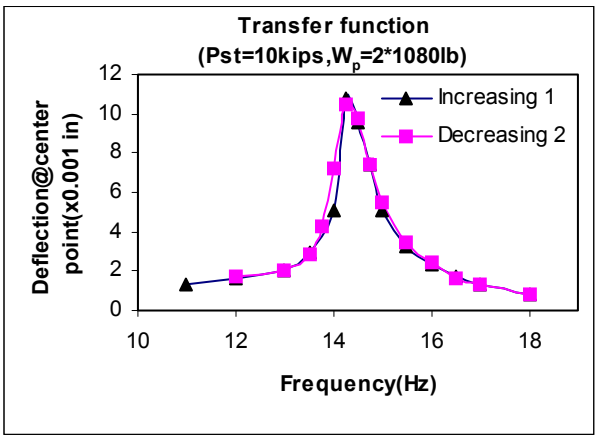
Transfer function
(Pst=10kips,Wp=2*1080lb)
Deflection@center point(x0.001 in)
Frequency(Hz)
Increasing 1
Decreasing 2
0
2
4
6
8
10
12
10
12
14
16
18

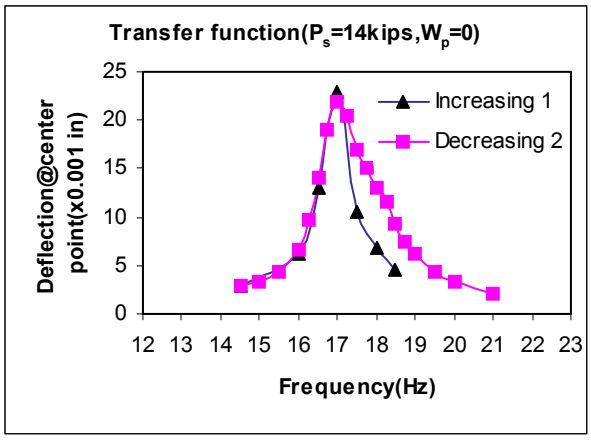
Transfer function(P_s=14kips,W_p=0)
Deflection@center point(x0.001 in)
Frequency(Hz)
Increasing 1
Decreasing 2
0
5
10
15
20
25
12 13 14 15 16 17 18 19 20 21 22 23

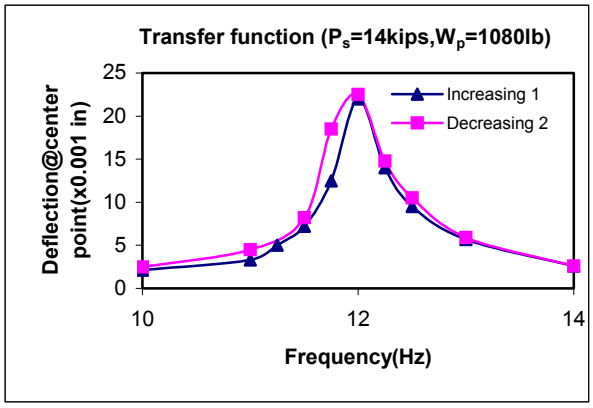
Transfer function (P_s=14kips,W_p=1080lb)
Deflection@center point(x0.001 in)
Frequency(Hz)
Increasing 1
Decreasing 2
0
5
10
15
20
25
10
12
14

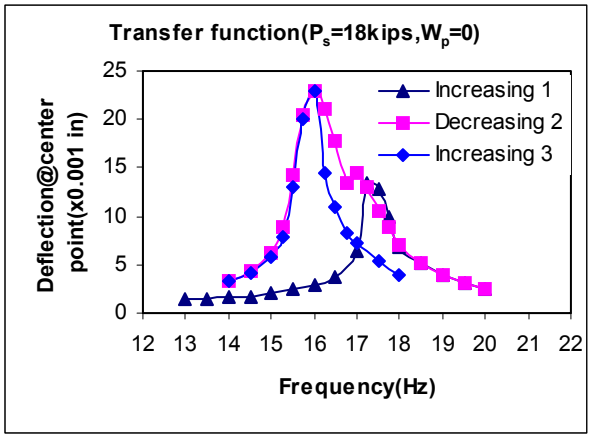
Transfer function(P_s=18kips,W_p=0)
Deflection@center point(x0.001 in)
Frequency(Hz)
Increasing 1
Decreasing 2
Increasing 3
0
5
10
15
20
25
12 13 14 15 16 17 18 19 20 21 22

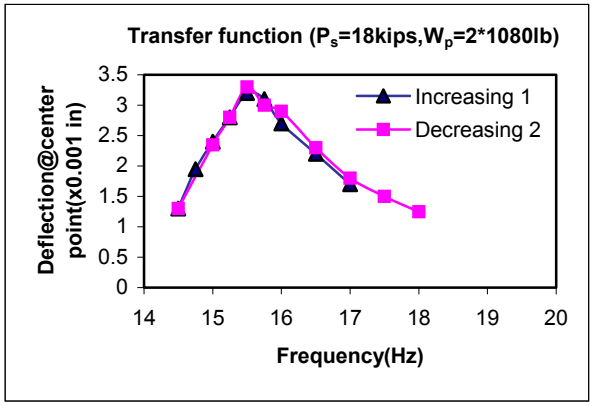
Transfer function (P_s=18kips,W_p=2*1080lb)
Deflection@center point(x0.001 in)
Frequency(Hz)
Increasing 1
Decreasing 2
3.5
3
2.5
2
1.5
1
0.5
0
14
15
16
17
18
19
20

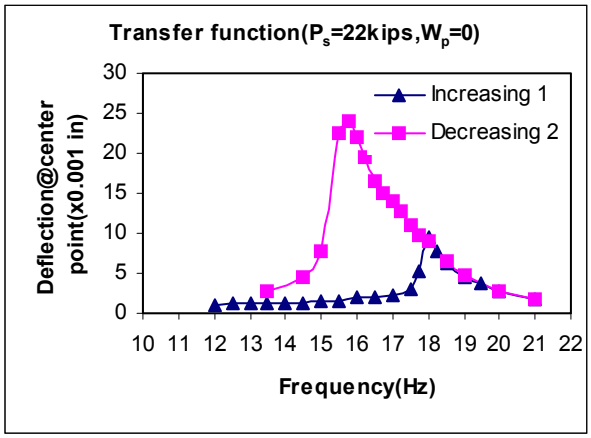
Transfer function(P_s=22kips,W_p=0)
Deflection@center point(x0.001 in)
Frequency(Hz)
Increasing 1
Decreasing 2
30
25
20
15
10
5
0
10 11 12 13 14 15 16 17 18 19 20 21 22

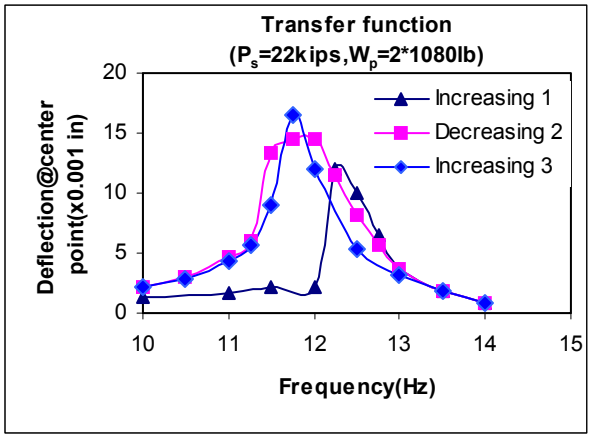
Transfer function
(P_s=22kips,W_p=2*1080lb)
Deflection@center point(x0.001 in)
Frequency(Hz)
Increasing 1
Decreasing 2
Increasing 3
20
15
10
5
0
10 11 12 13 14 15

APPENDIX C:

TRANSFER FUNCTIONS OF BEAM 3

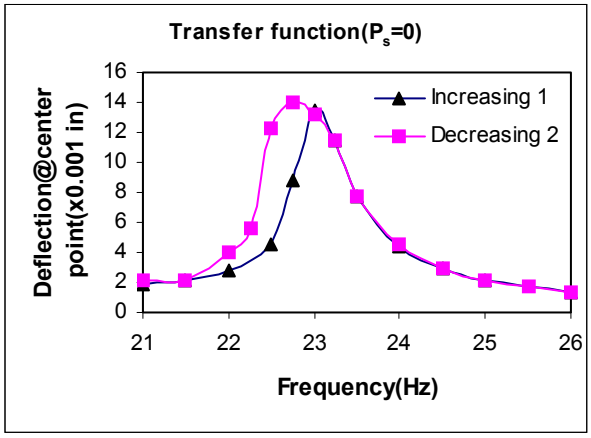
Transfer function(P_s=0)
Deflection@center point(x0.001 in)
Frequency(Hz)
Increasing 1
Decreasing 2
0
2
4
6
8
10
12
14
16
21
22
23
24
25
26

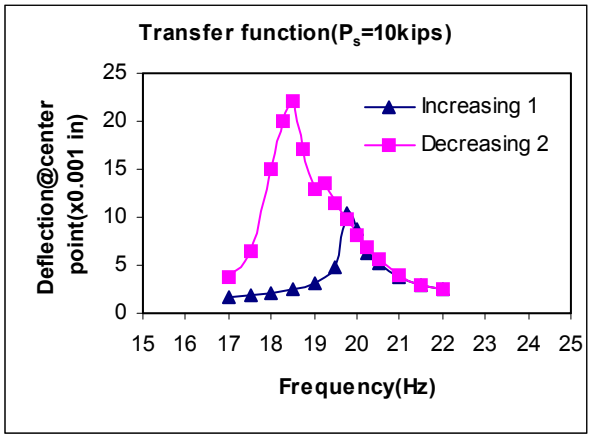
Transfer function(P_s=10kips)
Deflection@center point(x0.001 in)
Frequency(Hz)
Increasing 1
Decreasing 2
0
5
10
15
20
25
15
16
17
18
19
20
21
22
23
24
25

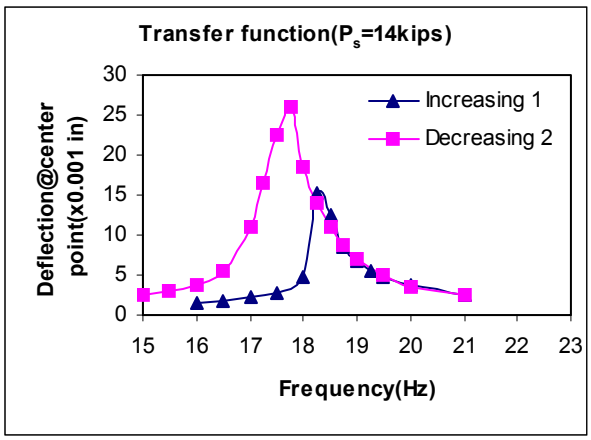
Transfer function(P_s=14kips)
Deflection@center point(x0.001 in)
Frequency(Hz)
Increasing 1
Decreasing 2
0
5
10
15
20
25
30
15
16
17
18
19
20
21
22
23

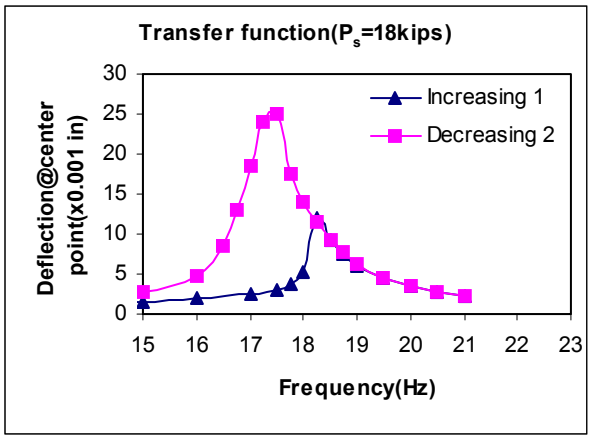
Transfer function(P_s=18kips)
Deflection@center point(x0.001 in)
Frequency(Hz)
Increasing 1
Decreasing 2
0
5
10
15
20
25
30
15
16
17
18
19
20
21
22
23

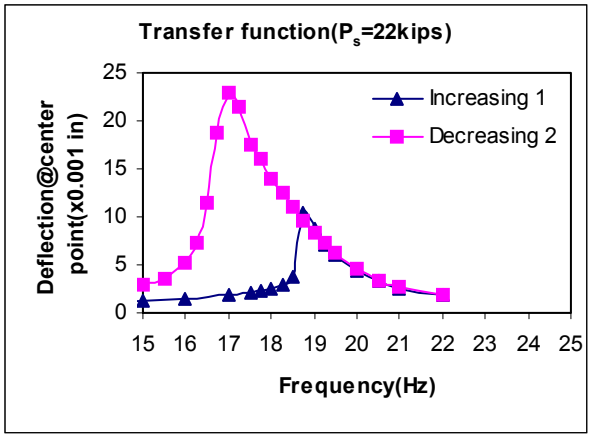
Transfer function(P_s=22kips)
Deflection@center point(x0.001 in)
Frequency(Hz)
Increasing 1
Decreasing 2
0
5
10
15
20
25
15
16
17
18
19
20
21
22
23
24
25

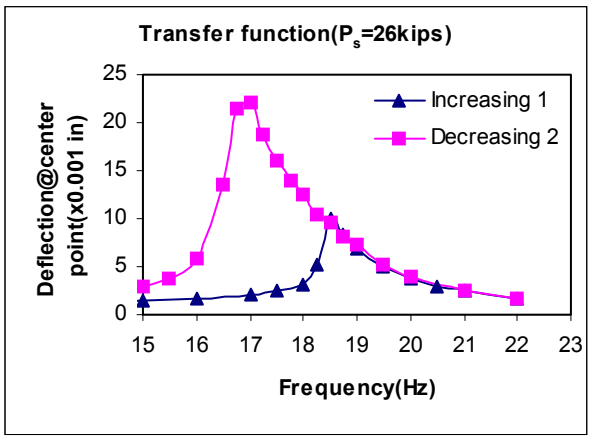
Transfer function(P_s=26kips)
Deflection@center point(x0.001 in)
Frequency(Hz)
Increasing 1
Decreasing 2
0
5
10
15
20
25
15
16
17
18
19
20
21
22
23

APPENDIX D:

TRANSFER FUNCTIONS OF BRIDGE J857

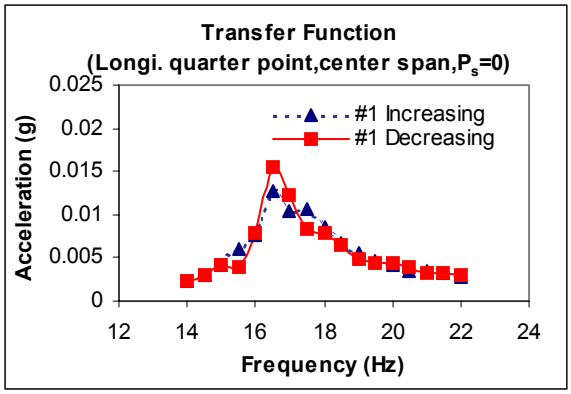
Transfer Function
(Longi. quarter point,center span,Ps=0)
Acceleration (g)
0.025
0.02
0.015
0.01
0.005
0
12
14
16
18
20
22
24
Frequency (Hz)
#1 Increasing
#1 Decreasing

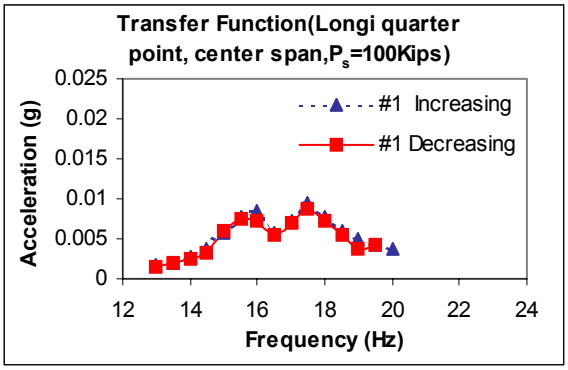
Transfer Function(Longi quarter
point, center span,Ps=100Kips)
Acceleration (g)
0.025
0.02
0.015
0.01
0.005
0
12
14
16
18
20
22
24
Frequency (Hz)
#1 Increasing
#1 Decreasing

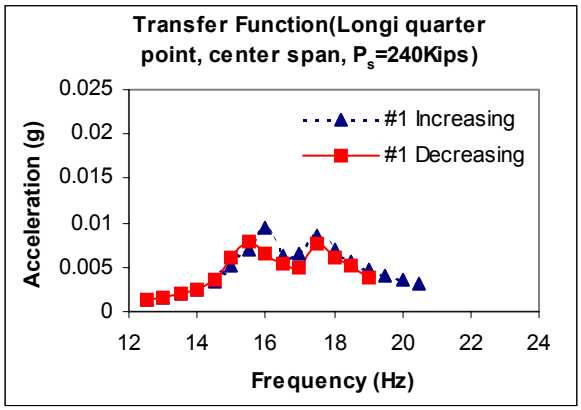
Transfer Function(Longi quarter
point, center span, Ps=240Kips)
Acceleration (g)
0.025
0.02
0.015
0.01
0.005
0
12
14
16
18
20
22
24
Frequency (Hz)
#1 Increasing
#1 Decreasing

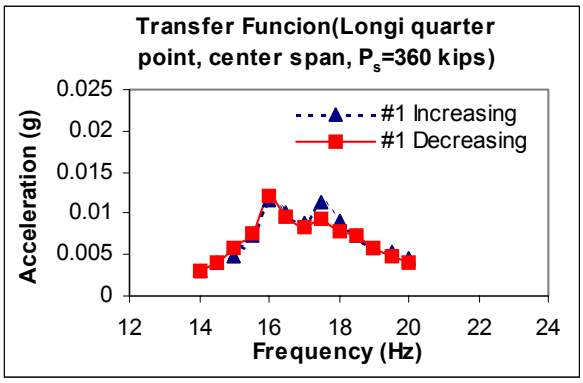
Transfer Funcion(Longi quarter point, center span, P_s=360 kips)
Acceleration (g)
0.025
0.02
0.015
0.01
0.005
0
12
14
16
18
20
22
24
Frequency (Hz)
#1 Increasing
#1 Decreasing

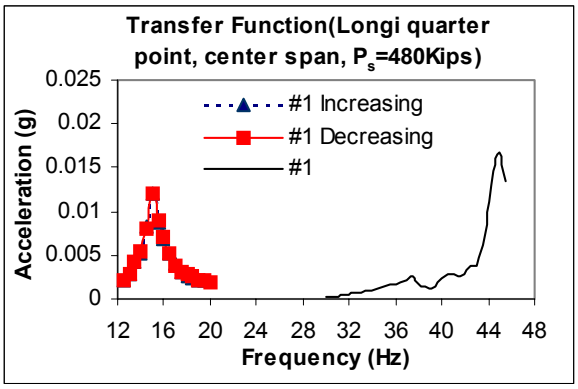
Transfer Function(Longi quarter point, center span, P_s=480Kips)
Acceleration (g)
0.025
0.02
0.015
0.01
0.005
0
12
16
20
24
28
32
36
40
44
48
Frequency (Hz)
#1 Increasing
#1 Decreasing
#1

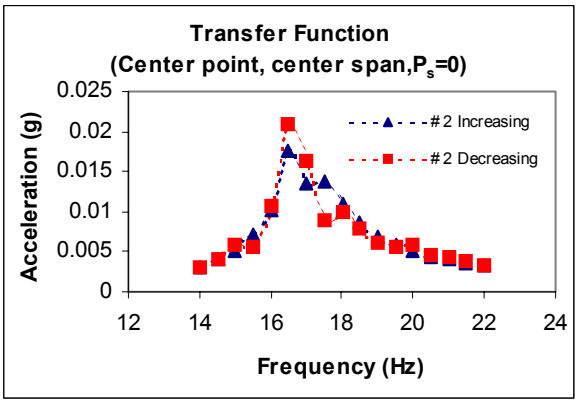
Transfer Function (Center point, center span,P_s=0)
Acceleration (g)
0.025
0.02
0.015
0.01
0.005
0
12
14
16
18
20
22
24
Frequency (Hz)
#2 Increasing
#2 Decreasing

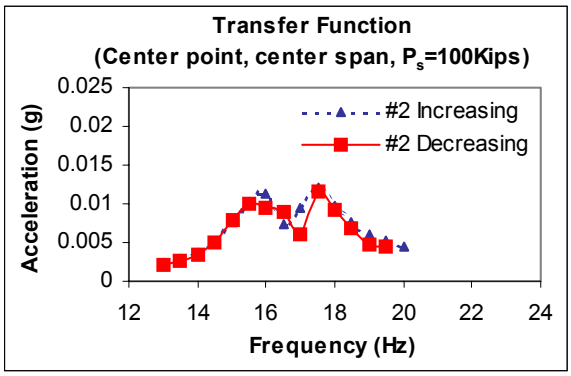
Transfer Function
(Center point, center span, P_s=100Kips)
Acceleration (g)
0.025
0.02
0.015
0.01
0.005
0
#2 Increasing
#2 Decreasing
12
14
16
18
20
22
24
Frequency (Hz)

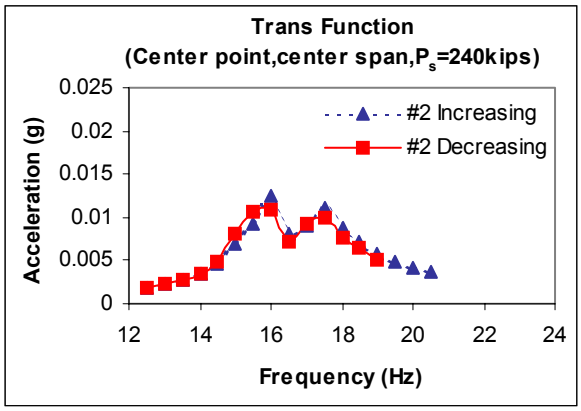
Trans Function
(Center point,center span,P_s=240kips)
Acceleration (g)
0.025
0.02
0.015
0.01
0.005
0
#2 Increasing
#2 Decreasing
12
14
16
18
20
22
24
Frequency (Hz)

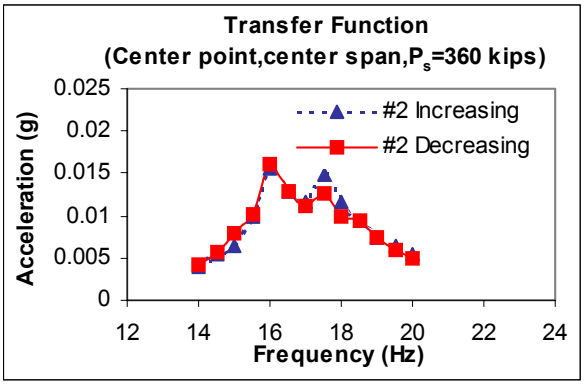
Transfer Function
(Center point,center span,P_s=360 kips)
Acceleration (g)
0.025
0.02
0.015
0.01
0.005
0
#2 Increasing
#2 Decreasing
12
14
16
18
20
22
24
Frequency (Hz)

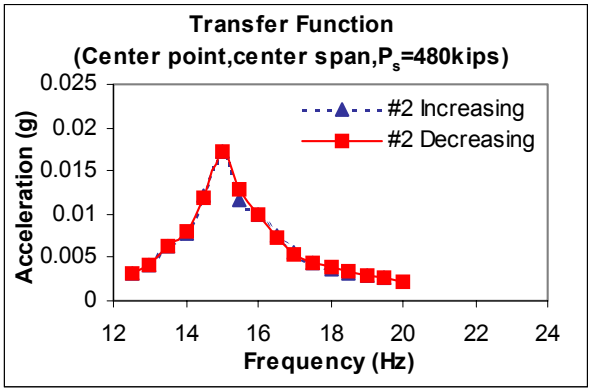
Transfer Function
(Center point,center span,P_s=480kips)
Acceleration (g)
0.025
0.02
0.015
0.01
0.005
0
12
14
16
18
20
22
24
Frequency (Hz)
#2 Increasing
#2 Decreasing

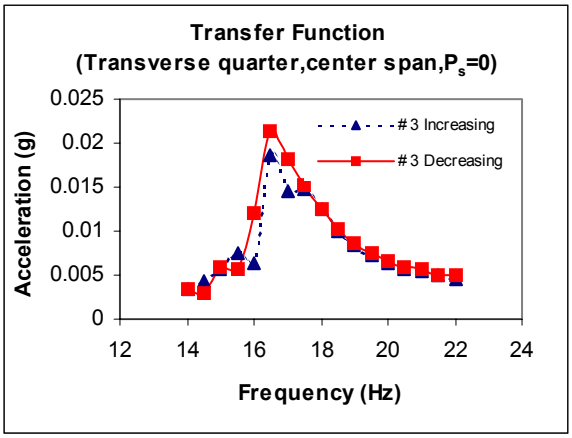
Transfer Function
(Transverse quarter,center span,P_s=0)
Acceleration (g)
0.025
0.02
0.015
0.01
0.005
0
12
14
16
18
20
22
24
Frequency (Hz)
#3 Increasing
#3 Decreasing

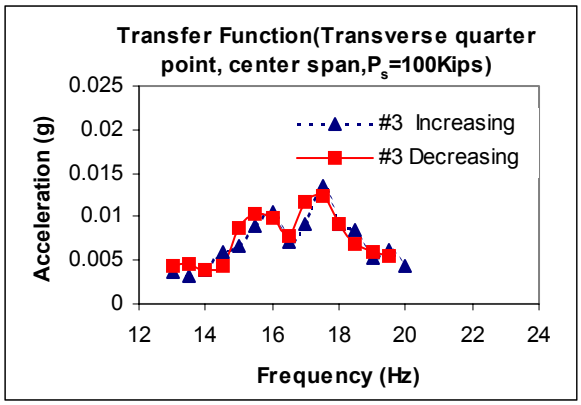
Transfer Function(Transverse quarter
point, center span,P_s=100Kips)
Acceleration (g)
0.025
0.02
0.015
0.01
0.005
0
12
14
16
18
20
22
24
Frequency (Hz)
#3 Increasing
#3 Decreasing

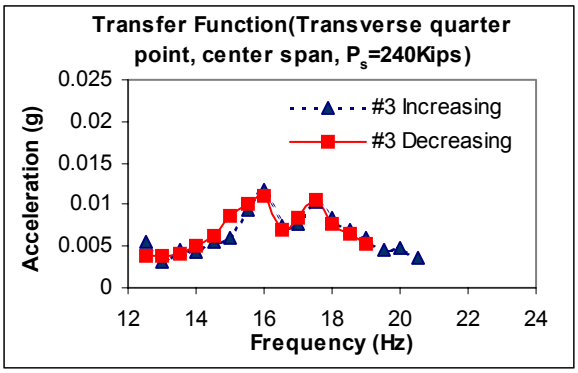
Transfer Function(Transverse quarter point, center span, P_s=240Kips)
Acceleration (g)
0.025
0.02
0.015
0.01
0.005
0
12
14
16
18
20
22
24
Frequency (Hz)
#3 Increasing
#3 Decreasing

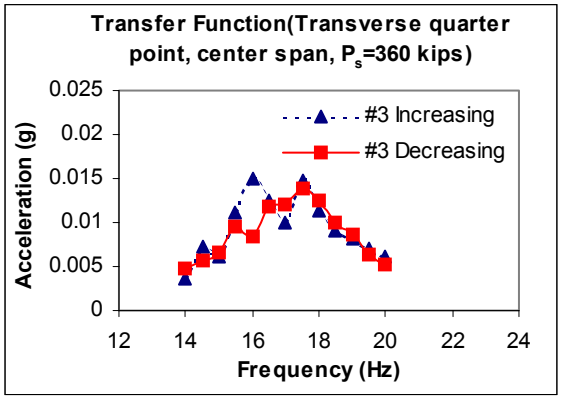
Transfer Function(Transverse quarter point, center span, P_s=360 kips)
Acceleration (g)
0.025
0.02
0.015
0.01
0.005
0
12
14
16
18
20
22
24
Frequency (Hz)
#3 Increasing
#3 Decreasing

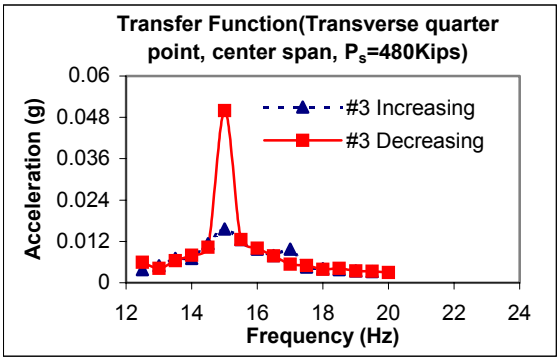
Transfer Function(Transverse quarter point, center span, P_s=480Kips)
Acceleration (g)
0.06
0.048
0.036
0.024
0.012
0
12
14
16
18
20
22
24
Frequency (Hz)
#3 Increasing
#3 Decreasing

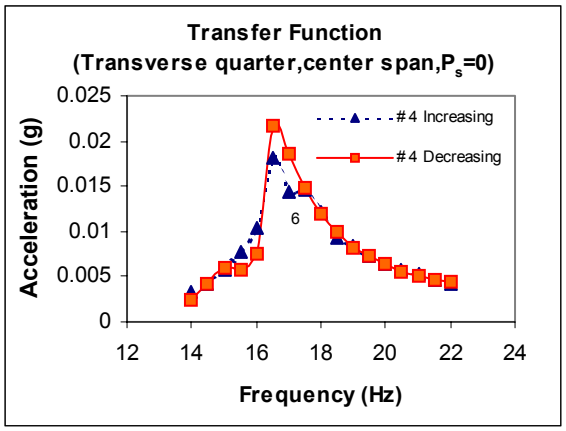
Transfer Function
(Transverse quarter,center span,P_s=0)
Acceleration (g)
0.025
0.02
0.015
0.01
0.005
0
12
14
16
18
20
22
24
Frequency (Hz)
#4 Increasing
#4 Decreasing
6

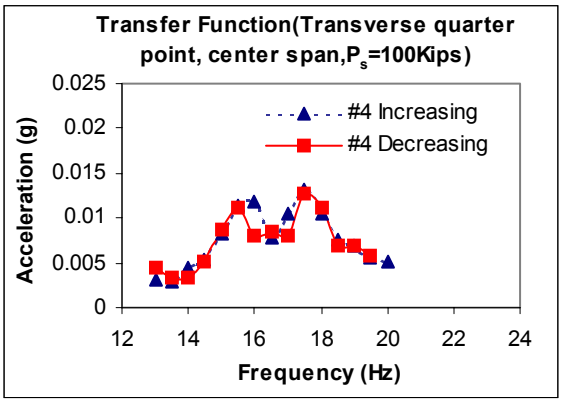
Transfer Function(Transverse quarter point, center span,P_s=100Kips)
Acceleration (g)
0.025
0.02
0.015
0.01
0.005
0
12
14
16
18
20
22
24
Frequency (Hz)
#4 Increasing
#4 Decreasing

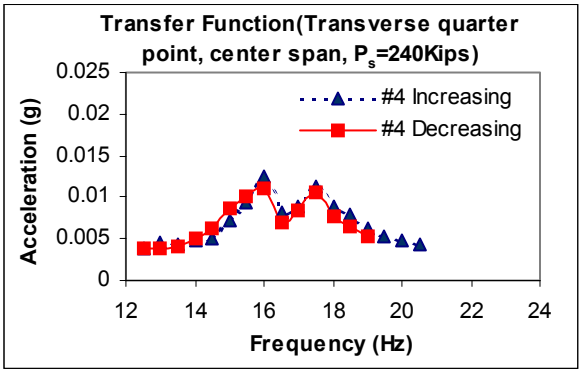
Transfer Function(Transverse quarter point, center span, P_s=240Kips)
Acceleration (g)
0.025
0.02
0.015
0.01
0.005
0
12
14
16
18
20
22
24
Frequency (Hz)
#4 Increasing
#4 Decreasing

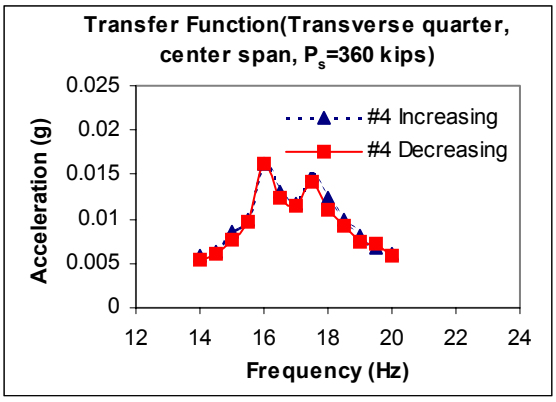
Transfer Function(Transverse quarter, center span, P_s=360 kips)
Acceleration (g)
0.025
0.02
0.015
0.01
0.005
0
12
14
16
18
20
22
24
Frequency (Hz)
#4 Increasing
#4 Decreasing

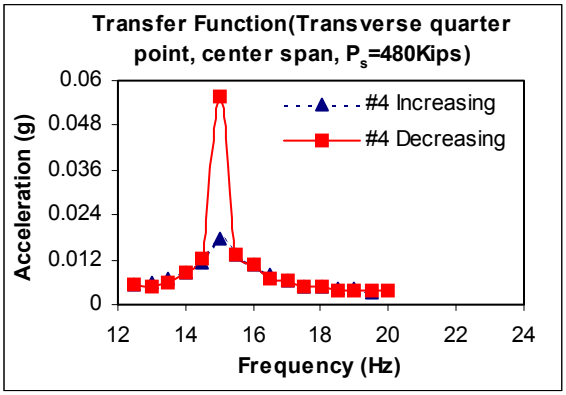
Transfer Function(Transverse quarter point, center span, P_s=480Kips)
Acceleration (g)
0.06
0.048
0.036
0.024
0.012
0
12
14
16
18
20
22
24
Frequency (Hz)
#4 Increasing
#4 Decreasing

APPENDIX E:

TRANSFER FUNCTIONS OF BEAM 2 FROM SWEPT-SINE TESTS

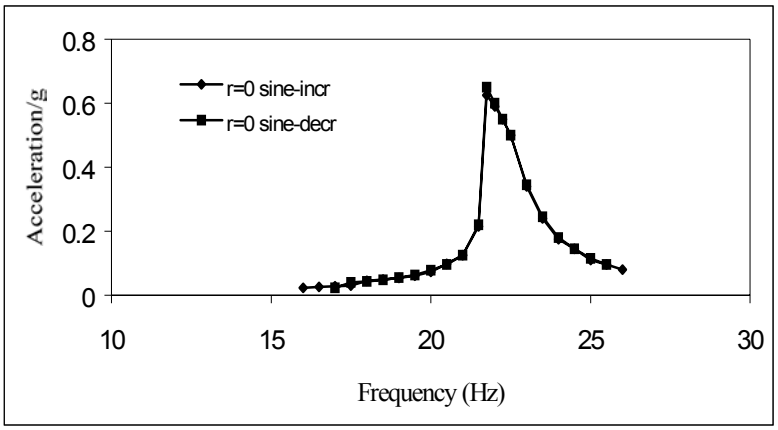
0.8
0.6
0.4
0.2
0
Acceleration/g
r=0 sine-incr
r=0 sine-decr
10
15
20
25
30
Frequency (Hz)

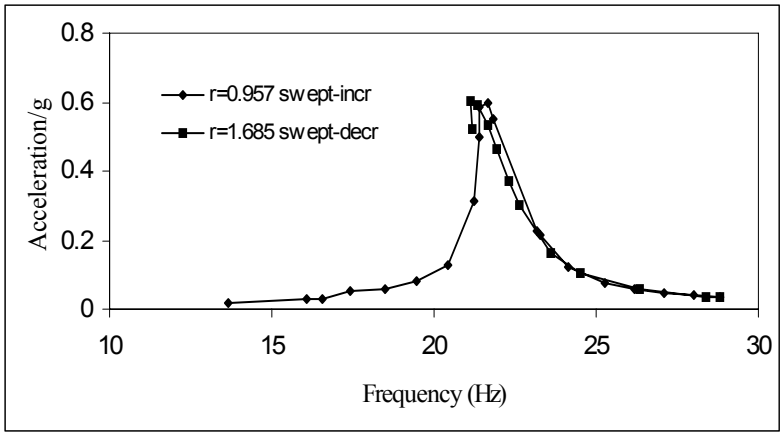
0.8
0.6
0.4
0.2
0
Acceleration/g
r=0.957 swept-incr
r=1.685 swept-decr
10
15
20
25
30
Frequency (Hz)

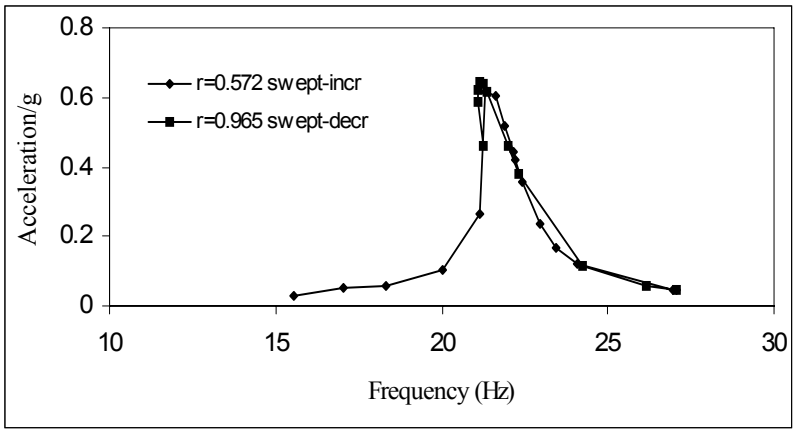
0.8
0.6
0.4
0.2
0
Acceleration/g
r=0.572 swept-incr
r=0.965 swept-decr
10
15
20
25
30
Frequency (Hz)

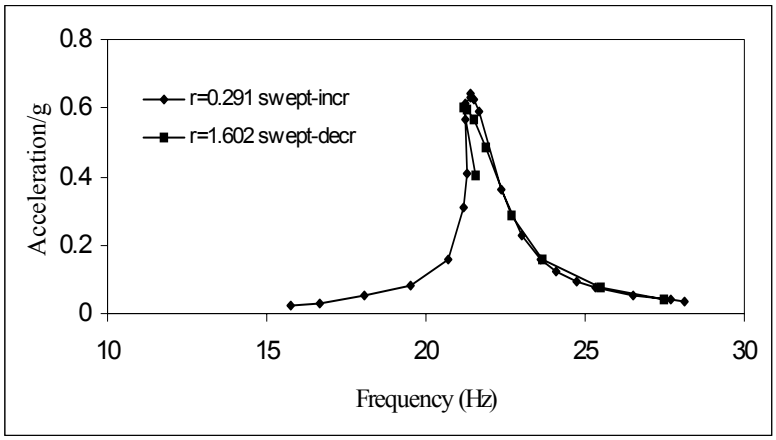
0.8
0.6
0.4
0.2
0
Acceleration/g
r=0.291 swept-incr
r=1.602 swept-decr
10
15
20
25
30
Frequency (Hz)

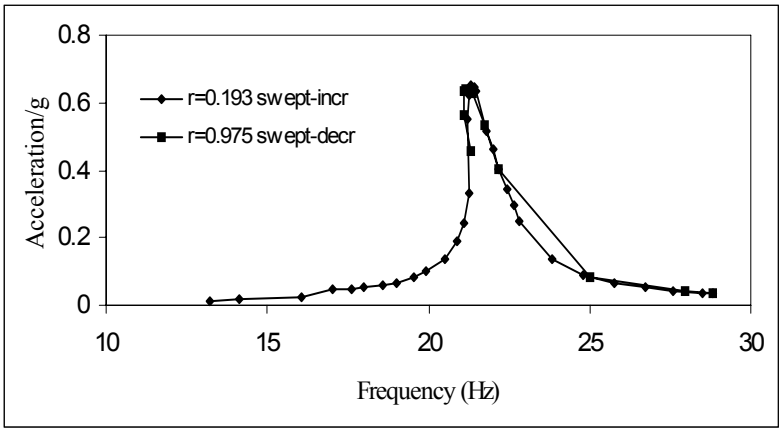
0.8
0.6
0.4
0.2
0
Acceleration/g
r=0.193 swept-incr
r=0.975 swept-decr
10
15
20
25
30
Frequency (Hz)

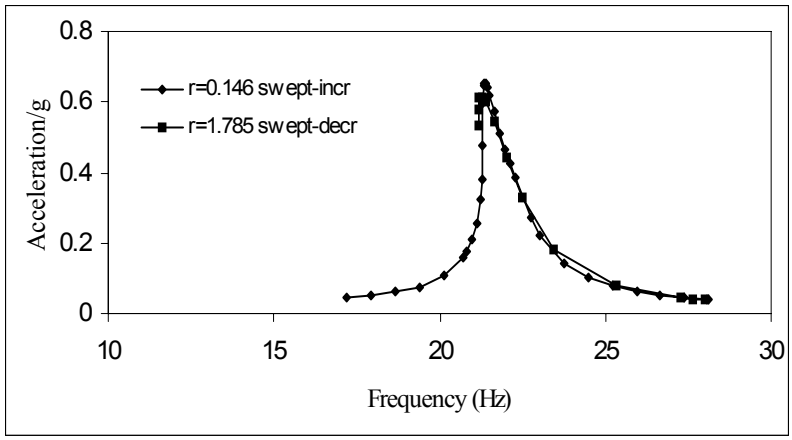
0.8
0.6
0.4
0.2
0
Acceleration/g
r=0.146 swept-incr
r=1.785 swept-decr
10
15
20
25
30
Frequency (Hz)

APPENDIX F:

TRANSFER FUNCTIONS OF BEAM 3 FROM SWEPT-SINE TESTS

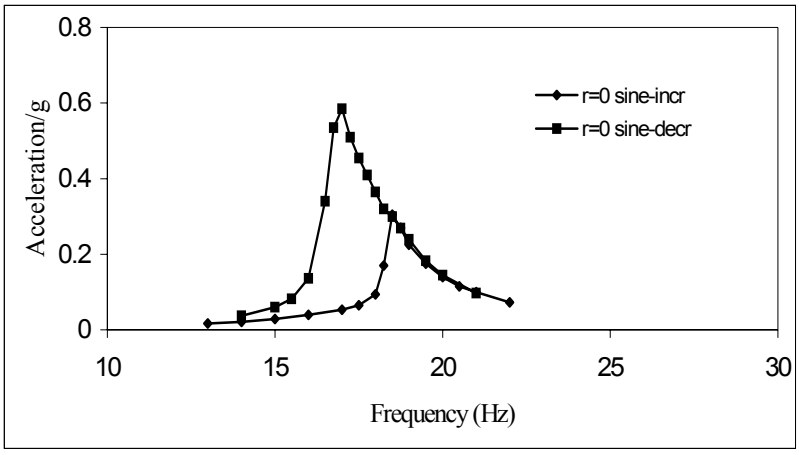
0.8
0.6
0.4
0.2
0
Acceleration/g
r=0 sine-incr
r=0 sine-decr
10
15
20
25
30
Frequency (Hz)

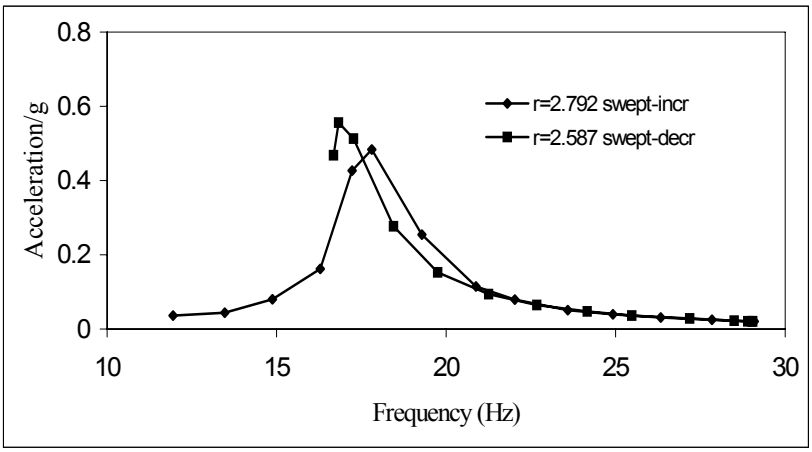
0.8
0.6
0.4
0.2
0
Acceleration/g
r=2.792 swept-incr
r=2.587 swept-decr
10
15
20
25
30
Frequency (Hz)

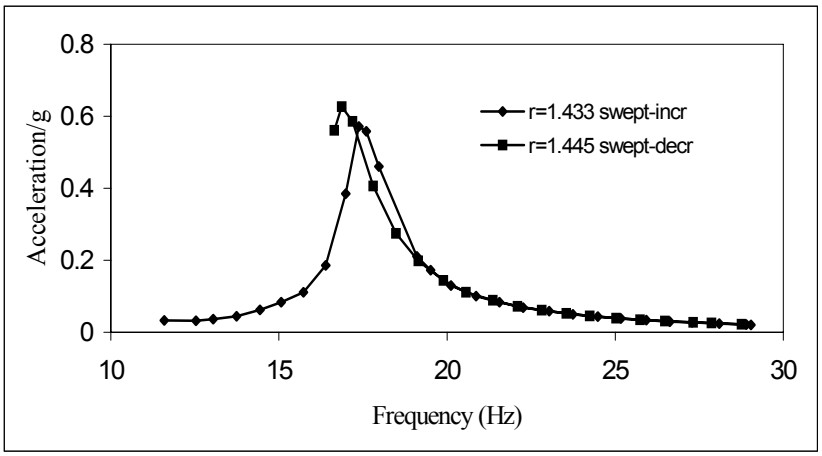
0.8
0.6
0.4
0.2
0
Acceleration/g
r=1.433 swept-incr
r=1.445 swept-decr
10
15
20
25
30
Frequency (Hz)

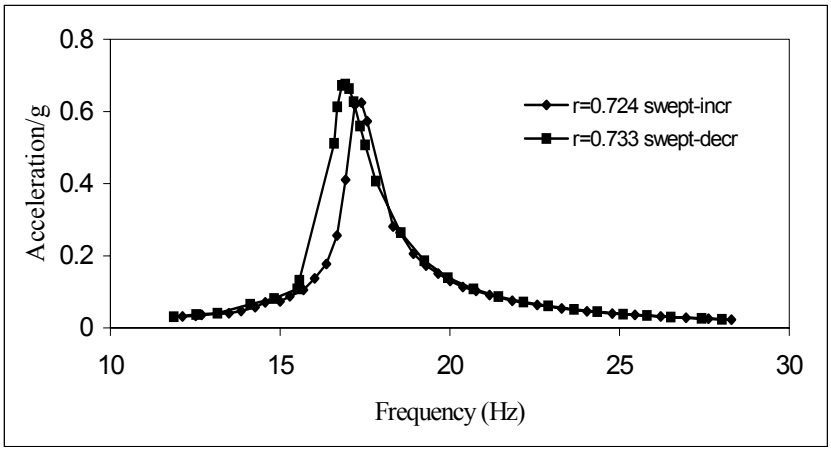
0.8
0.6
0.4
0.2
0
Acceleration/g
r=0.724 swept-incr
r=0.733 swept-decr
10
15
20
25
30
Frequency (Hz)

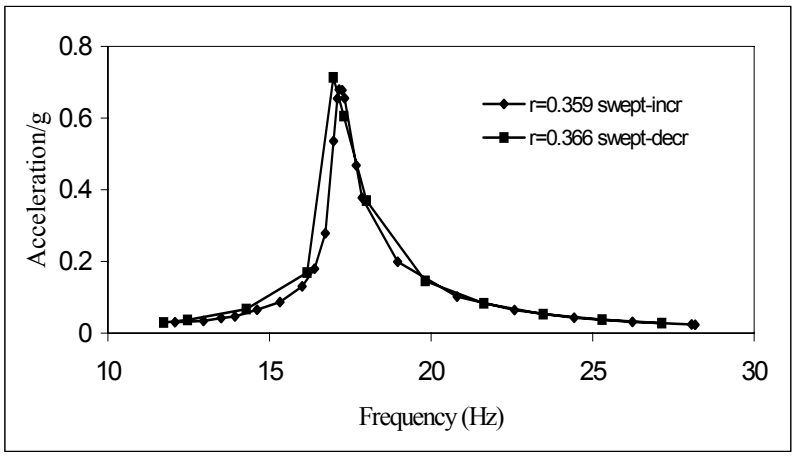
0.8
0.6
0.4
0.2
0
Acceleration/g
r=0.359 swept-incr
r=0.366 swept-decr
10
15
20
25
30
Frequency (Hz)

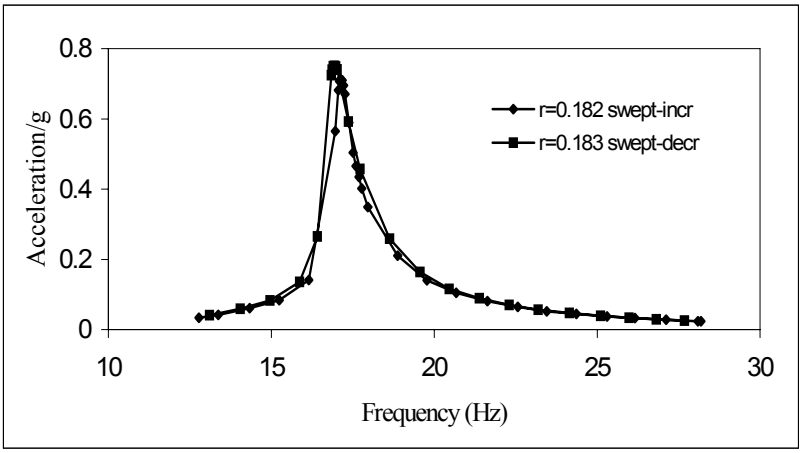
0.8
0.6
0.4
0.2
0
Acceleration/g
r=0.182 swept-incr
r=0.183 swept-decr
10
15
20
25
30
Frequency (Hz)

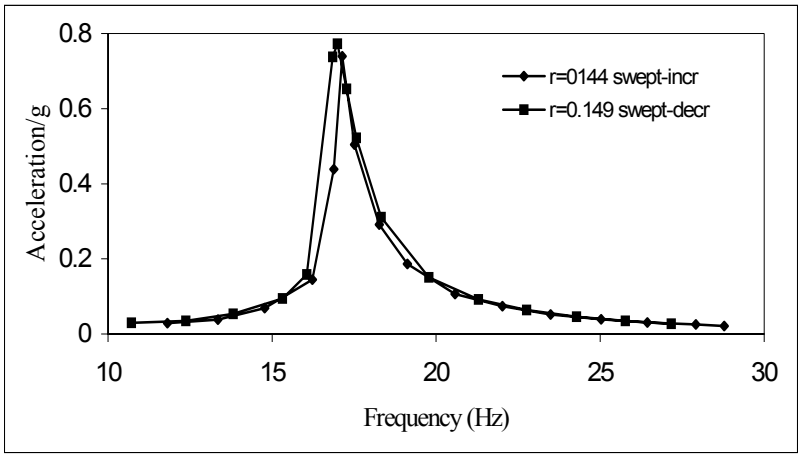
0.8
0.6
0.4
0.2
0
Acceleration/g
10
15
20
25
30
Frequency (Hz)
r=0144 swept-incr
r=0.149 swept-decr